Delft University of Technology

Doppler Spectrum Parameter Estimation for Weather Radar Echoes Using a Parametric Semianalytical Model

Dash, Tworit ; Driessen, Hans; Krasnov, Oleg A.; Yarovoy, Alexander

Important note
To cite this publication, please use the final published version (if applicable).
Please check the document version above.

Doppler Spectrum Parameter Estimation for Weather Radar Echoes Using a Parametric Semianalytical Model

Tworit Dash, *Graduate Student Member, IEEE*, Hans Driessen,
Oleg A. Krasnov, and Alexander Yarovoy, *Fellow, IEEE*

Abstract— **The problem of the limited accuracy of precipitation Doppler spectrum moments estimation measured by fast azimuthally scanning weather radars is addressed. A novel approach for the Doppler moment estimation based on maximum likelihood estimation is proposed. A simplified semianalytical parametric model for the precipitation power spectral density (PSD) as a function of the velocity parameters of the scatterers and the finite radar observation time is derived for typical precipitation-like weather conditions. An inverse problem for estimating the Doppler moments from measurements of the PSD is formulated and solved. It is demonstrated that the variance of the estimation of the Doppler moments approaches the Cramer Rao Lower Bound (CRB) when the observation time approaches infinity. The performance of the proposed approach is compared with some classical techniques and another realization of the maximum likelihood approach based on simulated and experimental data. The results indicate the superiority of the proposed approach, especially for short observation time. Furthermore, a scanning strategy to accurately estimate the Doppler moments based on the true velocity dispersion of the scatterers is provided with the help of the proposed approach.**

Index Terms— **Doppler velocity retrieval, parametric spectrum estimation, radar signal processing.**

I. INTRODUCTION

DOPPLER weather radars are primarily used to detect precipitation, estimate the motion of raindrops, and classify the hydrometeors (rain, hail, graupel, and snow) in the atmosphere. This information helps us understand the severity of storms and the microphysics of the hydrometeors. Our focus is on retrieving the Doppler parameters, which help in the abovementioned applications.

Traditionally, three Doppler parameters (also known as the Doppler moments) are retrieved from the echoes received by the radar to characterize the intensity and the motion of the raindrops. The first parameter is the total power contained in the backscattered radar signal (also known as the zeroth

Doppler moment), and it is used to detect the presence of precipitation.

The other two parameters help determine the motion of the raindrops and are derived from the phase change of these echoes in time. The mean Doppler velocity (also known as the first Doppler moment) is a measure of the mean radial velocity of the raindrops. The spatial and temporal variability of the mean Doppler velocity helps determine the horizontal wind field (speed and direction of the wind as a function of space and time) and the mean vertical fall velocity of the raindrops [1], [2], [3], [4], [5], [6], [7].

The Doppler spectrum width (the square root of the second spectral Doppler moment about the mean velocity, i.e., the second central moment) is a measure of velocity dispersion associated with several statistical effects such as wind shear, turbulence, as well as antenna beam shape. The Doppler spectrum width is used mainly to estimate the turbulence intensity field in the atmosphere [8], [9], [10], [11], [12], and the drop size distribution (DSD) of the raindrops [13], [14], [15], [16], [17]. The use of Doppler moments can also be found in fields of study other than weather radars, such as ultrasonic Doppler blood flow sensing [18] and radar astronomy [19], [20].

The classical Doppler moment estimators need long records of the echo samples to estimate the moments accurately (especially for the Doppler spectrum width), for which it is assumed that the spectral content is constant for a long observation time (stationarity condition). However, the stationarity condition is often not realized in practice due to, e.g., instability of the physical atmospheric conditions and rapid radar scans. A changing atmosphere is disadvantageous for slowly scanning traditional weather radars that can accumulate long records of echo samples. On the other hand, classical estimators give biased results in the case of rapidly scanning radars because of limited time on target [21].

In this article, we focus on the fast azimuthal scanning radars. Therefore, considering the stationarity condition of the atmosphere only for a short period, a desired moment estimator should have the feature to estimate the moments with a small observation time accurately. Another feature of this desired estimator is the ability to process the data from multiple radar scans. We propose a maximum likelihood estimator that has both the features mentioned above. In addition to that, we also propose a quantitative guide to how fast the radar should scan as a function of the true velocity dispersion.

The main body of this article is organized as follows. Section II discusses the classical estimators and the rationale behind the proposed approach. Section III explains the simplified time domain echo signal model for precipitation-like weather targets. Section IV contains the proposed semianalytical model of the power spectrum. Section V discusses the optimization goals of the approach and the formulation of the likelihood function for the parameter estimation. Section VI contains some examples of the estimation using simulated weather echoes, the comparison with the existing approaches, and the performance analysis. Section VII presents the application to real radar observations. The conclusions are mentioned in Section VIII. Appendix A contains the derivation of the expected semi-analytical model of the PSD. Appendix B contains the derivation of the theoretical variances (for any number of echo samples) and the unbiased CRB for the proposed approach (for infinite number of echo samples).

II. CLASSICAL DOPPLER MOMENT ESTIMATORS AND THE RATIONALE BEHIND THE PROPOSED APPROACH

The Doppler moments estimation techniques can be categorized into parametric and nonparametric approaches. The most common and classical nonparametric techniques used to estimate these moments are the periodogram-based (also called the power spectrum-based approach, which is referred to as DFT in this article) and the autocovariance (ACV)-based approach (also called the pulse pair method and referred as PP approach in this article). The performance analysis of such methods along with some other classical nonparametric estimators, such as the vector phase change (VPC) and the scalar phase change (SPC) has been studied in [21], [22], [23], and [24]. The DFT-based moment estimation is carried out after the reconstruction of the spectrum shape in the frequency domain and is sensitive to the Doppler spectrum resolution due to limited observation time. The moment estimates are asymptotically unbiased, meaning that the estimates converge to the true value when the number of coherent echo samples in time approaches infinity. The PP approach, on the other hand, is an unbiased estimator of the first moment provided the Doppler spectrum is symmetric around the mean Doppler velocity. Different versions of the PP approach exist for the spectrum width estimation that benefit from various combinations of the ACV of the echo samples with various numbers of sample lags [25], [26], [27, Ch. 6, pp. 136-138]. The different PP approaches are denoted as PP Rm/Rn, where Ri is the autocorrelation of the echo samples in the time domain with i number of sample lags. It has been shown in [25] and [26] that the PP approaches with higher lags perform superior for smaller spectrum widths and vice versa. A hybrid estimator is proposed in [26], where the estimator chooses one of the PP versions heuristically based on an initial estimate of the spectrum width. Moreover, a different version of the PP algorithm exists in the literature as poly pulse pair (PPP) [28] method for the first Doppler moment, but its discussion goes beyond the scope of this article. Another nonparametric approach [29] assumes the band-limited nature of the Doppler spectrum. Although its accuracy is better than the DFT and PP approaches, it is based on estimating interpolation-filter coefficients. The choice of

the impulse transfer function of the filter is empirical and due to the need to estimate many filter coefficients, the approach becomes computationally expensive. Another nonparametric moment estimator class uses autoregressive moving average (ARMA) models [30]. However, fitting ARMA models also consumes considerable computational resources. Even though many nonparametric approaches for Doppler spectrum estimation exist in the literature, the DFT and PP approaches are the most popular because of their computational efficiency and nonparametric nature.

The parametric approaches assume a model for the echo samples' PSD or ACV. The maximum likelihood estimation using a power spectrum model of the weather echoes is studied in [31] and [32] and a maximum entropy-based approach is studied in [33]. These methods have the advantage of processing finite sequences of echo samples and gapped records (like that of a scanning radar). Although these techniques provide accurate results for the mean Doppler velocity, they give biased results when estimating the Doppler spectrum width due to the limited observation time. These estimators use a closed-form shape of the Doppler spectrum and do not consider the Doppler resolution. In [34], a Gaussian spectrum convolved with a rectangular window has been considered as a model of the PSD to remove the effect of the limited resolution. However, the deconvolution is performed manually after studying the bias in a tabular form, and analytical expressions are not known for the variance of the estimator.

In this article, we propose a novel approach, referred to later as a parametric spectrum estimator (PSE), to estimate Doppler spectrum moments accurately by processing several mutually incoherent finite sequences of echo samples. The method is based on a novel semianalytical model of the PSD, which is derived using a limited observation time and thus incorporates the Doppler resolution in the model. The PSD model is derived using a simplified physical model of the time domain signal similar to [35] with some changes in the model of the velocities of the raindrops.

In the signal model, the velocities of the scatterers are considered to be independent and identically distributed (i.i.d.) random variables. As the shape of the majority of the weather Doppler spectrum is Gaussian in nature [22], [23], [27, Ch. 5, pp. 112-115], [36], and, the velocities of the raindrops are assumed to be normally distributed having parameters μ_v as the mean of the distribution (true mean Doppler velocity) and σ_v as the standard deviation (true Doppler spectrum width). The model of the PSD is derived by taking the expectation of the power of the discrete Fourier transform of the time domain signal model. The resulting expression for the PSD is semianalytical with a numerical sum across the finite time interval with steps equal to the pulse repetition time of the radar. A maximum likelihood approach is used to obtain the spectrum parameters similar to [31]. The formulation of the signal model, along with the derivation of the PSD is presented in Sections III and IV.

The performance of this estimator is evaluated by comparing its variance with the other approaches, such as DFT, PP, and Levin's ML approach [31]. In addition, a quantitative guide to how fast a radar should scan the atmosphere as a function

of the true velocity dispersion is proposed. The approach is successfully applied to multiple scans of experimental data acquired by a fast-scanning atmospheric radar.

III. SIGNAL MODEL

This article focuses on the echo sample modeling of weather radar in the context of precipitation-like events only. Consider a radar resolution volume filled with M raindrops during a rain event. The radar echo at time k is a superposition of the echoes received from all the raindrops [27, Ch. 4, p. 67]. It is given by

$$s(t_k) = \sum_{m=1}^{M} A_m \exp\left(j\frac{4\pi}{\lambda} r_m(t_k)\right). \tag{1}$$

In (1), A_m is the amplitude caused by the reflection from the mth scatterer. It is usually a function of the geometry of the scatterers (size, shape, orientation, and composition), the range weighting function due to the effect of the radar waveform, and the antenna weighting function based on the antenna beam shape [27, Ch. 5, pp. 112-115], [35]. The quantity λ is the wavelength of the radar signal, r_m is the distance to the mth scatterer, and j is the imaginary unit $(-1)^{1/2}$. The change in a scatterer's radial distance depends on its radial velocity. If we consider the radial velocity of the m'th scatterer to be $v_{m,r}$ at the time instant t_{k-1}, the radial distance of the mth scatterer at time t_k becomes $r_m(t_k) = r_m(t_{k-1}) + v_{m,r}T$, where $T = t_k - t_{k-1}$ is the pulse repetition time for the radar. If we consider that the radial velocity of each scatterer is constant throughout the observation time, and if we denote the initial position of the m'th scatterer to be $r_{m,0}$, the expression in (1) could be rewritten as follows:

$$s(t_k) = \sum_{m=1}^{M} A_m \exp\left(j\frac{4\pi}{\lambda}\left(r_{m,0} + v_{m,r}(t_k - t_0)\right)\right). \tag{2}$$

If we consider the initial time instant to be $t_0 = 0$ and by using $\beta_m = (4\pi/\lambda)r_{m,0}$, (2) could be rewritten as follows:

$$s(t_k) = \sum_{m=1}^{M} A_m \exp(j\beta_m) \exp\left(j\frac{4\pi}{\lambda} v_{m,r}t_k\right) \tag{3}$$

where the term $\exp(j\beta_m)$ is the initial phase caused by the incident phase of the electromagnetic wave (related to the transmit phase, range to resolution volume, and atmospheric affects) and the position of the mth scatterer relative to the center of the resolution volume. In this article, several assumptions have been considered for mathematical simplicity. The first assumption is that the sizes of the scatterers (raindrops) are assumed to be the same ($A_m = A \forall m$). The initial positions of the scatterers are $i.i.d.$ random variables with a uniform distribution

$$\{\beta_m\}_{m=1}^{M} \overset{i.i.d.}{\sim} \mathcal{U}[-\pi, \pi]. \tag{4}$$

We assume that the Gaussian shape of the Doppler spectrum around the mean Doppler velocity is caused purely by the scatterers' motion and not by other statistical effects explained in the introduction for mathematical convenience. The radial

velocities of the scatterers are considered $i.i.d.$ random variables with a Gaussian probability density

$$\{v_{m,r}\}_{m=1}^{M} \overset{i.i.d.}{\sim} \mathcal{N}(\mu_v, \sigma_v^2). \tag{5}$$

The time domain measurement model considered in this article includes the signal (3) with added zero mean complex white Gaussian noise with variance σ_n^2 and is given by

$$\mathbf{z} = \mathbf{s} + \mathbf{n}, \quad \{n_k\}_{k=0}^{N-1} \overset{i.i.d.}{\sim} \mathcal{CN}(0, \sigma_n^2). \tag{6}$$

IV. SEMIANALYTICAL FORM OF THE PSD

The signal model of (3) is used to derive the semi-analytical form of the PSD. Considering uniform sampling with pulse repetition interval of T, the DFT at a velocity point v can be represented as follows:

$$S(v) = A \sum_{k=0}^{N-1} \sum_{m=1}^{M} \exp\left[j\left(\frac{4\pi T}{\lambda}\left(v_{m,r} - v\right)k + \beta_m\right)\right]. \tag{7}$$

Performing the sum with respect to the time (summing a geometric progression) results in the following expression:

$$S(v) = A \sum_{m=1}^{M} \frac{\sin\left(\frac{2\pi T}{\lambda}N\left(v_{m,r} - v\right)\right)}{\sin\left(\frac{2\pi T}{\lambda}\left(v_{m,r} - v\right)\right)}$$
$$\times \exp\left[j(N-1)\left(v_{m,r} - v\right)\frac{2\pi T}{\lambda} + \beta_m\right] \tag{8}$$

where $\sin((2\pi T/\lambda)N(v_{m,r} - v))/\sin((2\pi T/\lambda)(v_{m,r} - v))$ (8) is a result of the finite observation time. This function is also called the Dirichlet kernel [37, Ch. 8, p. 189]. As we assume that the β are uniformly distributed phase, the expectations of the real and imaginary parts of (8) are 0 when $M \to \infty$. However, the PSD of the spectrum function of (8) does have a positive expectation. The PSD using (8) can be represented as follows:

$$|S(v)|^2/N$$
$$= A^2/N \left(\sum_{m=1}^{M} \frac{\sin^2\left((2\pi T/\lambda)N\left(v_{m,r} - v\right)\right)}{\sin^2\left((2\pi T/\lambda)\left(v_{m,r} - v\right)\right)} \right.$$
$$+ \sum_{p \neq q}^{M} \frac{\sin\left((2\pi T/\lambda)N\left(v_{p,r} - v\right)\right)}{\sin\left((2\pi T/\lambda)\left(v_{p,r} - v\right)\right)} \frac{\sin\left((2\pi T/\lambda)N\left(v_{q,r} - v\right)\right)}{\sin\left((2\pi T/\lambda)\left(v_{q,r} - v\right)\right)}$$
$$\left. \times \cos\left[(N-1)\left(v_{p,r} - v_{q,r}\right)(2\pi T/\lambda) + \left(\beta_p - \beta_q\right)\right] \right) \tag{9}$$

where the expectation of the second term is 0 because of the uniformly distributed β inside the cosine term. A detailed explanation of these two terms and their contribution to receiver power can be found in [27, Ch. 4, pp. 67-68]. Finally, the following expression gives the expectation of the first term, and the detailed derivation is presented in Appendix A

$$F(v) = \mathbb{E}\left[\frac{1}{N}|S(v)|^2\right]$$
$$= A^2 M \left[1 + 2\sum_{q=1}^{N-1}\left(1 - \frac{q}{N}\right)\exp\left(-\left(\frac{4\pi T}{\lambda}\right)^2 \frac{\sigma_v^2 q^2}{2}\right)\right.$$

$$\times \cos\left(\frac{4\pi T}{\lambda} q (\mu_v - v)\right)\bigg]. \qquad (10)$$

The dependence on N in the model is advantageous, especially for estimating the Doppler spectrum width, because parameter is heavily affected by the limited resolution of the spectrum. This makes it different from the existing maximum likelihood estimators, where a complete closed form of the PSD is used without the dependence of N.

V. OPTIMIZATION GOALS

The expression of (10) suggests that the PSD is a function of the spectrum parameters (the mean frequency (velocity, μ_v), the spectrum width σ_v), the finite number of coherent samples N, and the multiplicative factor $A^2 \times M$. As the multiplicative factor is a measure of the signal power, it can be estimated by taking the average of the signal power in the time domain

$$\hat{A}'^2 \approx \overline{|\mathbf{z}|^2}. \qquad (11)$$

Here, a change of parametrization is used for $A^2 M$ and is indicated as A'^2. The notation $\hat{A}'$ is used to suggest that it is an estimated quantity. In the following analysis, however, the value of A' is assumed to be known beforehand. The objective of the optimization here is to estimate the parameters $\Theta = [\mu_v, \sigma_v]$ based on the given PSD (the PSD of $\mathbf{z}$ is referred to as $\mathbf{Z}$).

Let us denote the number of observations of the PSD as L. Each of the L observations contains the PSD of N coherent radar echoes. However, the observations themselves need not be coherent. If the power spectrum is denoted by $Z_l(v)$ for lth observation, at a velocity point v, the likelihood probability is given by the following expression [31], [32]:

$$p(\mathbf{Z}|\Theta)$$
$$= \prod_{i=1}^{N} \prod_{l=1}^{L} \frac{1}{\pi \left(F(v_i, \Theta) + \sigma_n^2\right)} \exp\left(-\frac{Z_l(v_i)}{F(v_i, \Theta) + \sigma_n^2}\right) \quad (12)$$

where $p(\mathbf{Z}|\Theta)$ is the likelihood probability of $\mathbf{Z}$ given the parameters Θ. Here, $\mathbf{Z}$ is a matrix of size $L \times N$. This likelihood function is inspired by the fact that the probability density function of the PSD at a particular frequency (velocity) is exponential, indicating that the mean of the PSD is equal to its standard deviation [38]

$$Z(v_i) \sim \text{Exp}\left[\frac{1}{F(v_i) + \sigma_n^2}\right]. \qquad (13)$$

The following expression gives the logarithm of this likelihood function. In this formulation, the noise variance σ_n^2 is considered to be known

$$\log(p(\mathbf{Z}|\Theta))$$
$$= -\sum_{i=1}^{N} \left[L \log\left(\pi \left(F(v_i, \Theta) + \sigma_n^2\right)\right) + \frac{\sum_{l=1}^{L} Z_l(v_i)}{F(v_i, \Theta) + \sigma_n^2} \right]. \qquad (14)$$

The optimization aims at maximizing this log-likelihood (14) function to estimate the parameters Θ

$$\hat{\Theta} = \max_{\Theta} \log(p(\mathbf{Z}|\Theta)). \qquad (15)$$

The theoretical variances are computed for PSE and Levin's ML approaches by the following [31, eq. (4)]. The derivation of the theoretical variances is given in Appendix B. These theoretical variances can be computed for a finite number of samples. The biased-CRBs can also be derived for a finite number of samples [31, eq. (2)] by using the bias gradients of the parameters. However, the biases of these estimators are not known in closed form, making it challenging to obtain the biased-CRB for a finite number of samples. Nevertheless, it is essential to note that the theoretical variances for the infinite number of echo samples ($N \to \infty$, and for a fixed L) reach the unbiased-CRB (also referred to as CRB) as the estimators are asymptotically unbiased. Furthermore, the biased-CRB for the variances can be derived for biased estimators [39] by Bayesian inference (without having the bias gradients for the parameters in closed form). However, it is beyond the scope of this article.

In (14), it can be noticed that the likelihood function can integrate multiple observations (L in the expressions) of the stationary stochastic signal PSD. However, the existing classical nonparametric techniques only process one observation for the Doppler moment estimation, except for the DFT approach when periodogram smoothing is applied. The moment estimation with the DFT approach can be carried out after applying a periodogram smoothing technique on several realizations of the PSD (e.g., the periodogram of Bartlett and Welch [40, Ch. 4, pp. 49-52]) at the expense of poor Doppler resolution and hence is out of the scope of this article. In the simulation study, to have comparable results with DFT and PP, L is kept as 1, suggesting that only one observation (6) is processed in the proposed method and the classical methods. The optimization is performed using the active-set and the Limited Memory Broyden-Fletcher-Goldfarb-Shanno (L-BFGS) algorithms [41], [42]. This method is chosen for its faster computation time.

VI. NUMERICAL SIMULATION

This section applies the Doppler moment estimation on simulated radar echo samples. First, the noise-free echo samples are simulated using (3). A complex white Gaussian noise is added to the samples as shown in (6). The input noise variance for the measurement model is computed with a user-defined input SNR [38]. The PSE parameter estimation is compared with the DFT, PP, and Levin's ML approach. For all these approaches, the noise variance is assumed to be known to allow for a fair comparison. The expressions for moment estimation with the DFT approach using known noise variance are from [22, eq. (9)]. (The equation is for the mean Doppler, but similarly, the Doppler spectrum width is computed by using the second moment.) The mean Doppler estimation with the PP approach is taken from [22, eq. (16)]. For the Doppler spectrum width (PP R0/R1; also denoted as PP in this article, and PP R1/R2), the formulas [43, eq. (6.17) and eq. (6.32)] are used as these estimators are asymptotically unbiased. The formula [26, eq. (3)] is used for the $R1/R3$ spectrum width estimator.

For Levin's approach, the parameters are estimated jointly, like the PSE. The implementation of Levin's approach in
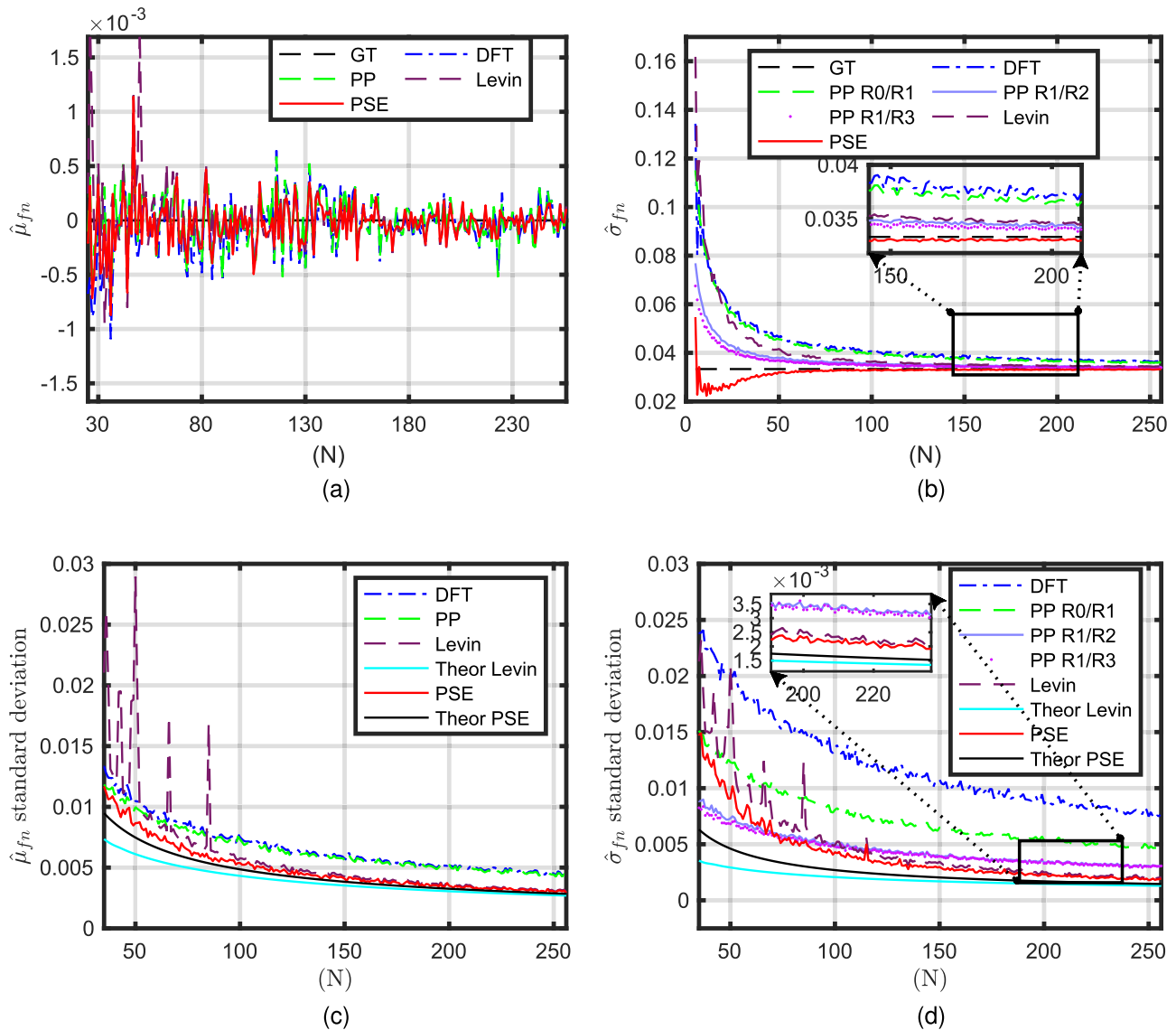
Fig. 1. Estimation and performance of the Doppler moments for $L = 1$ with respect to the number of coherent samples N: (a) mean normalized Doppler frequency $\hat{\mu}_{\text{fn}}$; (b) normalized Doppler frequency width $\hat{\sigma}_{\text{fn}}$; (c) standard deviation in estimating the normalized Mean Doppler frequency $\hat{\mu}_{\text{fn}}$; and (d) standard deviation in estimating the normalized Doppler spectrum width normalized $\hat{\sigma}_{\text{fn}}$.

this article differs from [31] in the sense that the continuous integrals are replaced with numerical sums along the frequencies, to include the effect of the limited frequency resolution. However, the implementation proposed in [31] assumes that the resolution is enough to contain the detailed structure of the spectrum, and also, it is assumed that the PSD is slowly varying (after applying some smoothing operation). Hence, in [31], continuous integrals along the frequencies are justified. However, to have a fair comparison of the PSE with Levin's approach, no smoothing operation has been performed on the PSD. Comparing the results of PSE with Levin's ML approach allows us to observe the differences between the estimates when using a model of the PSD has a semianalytical form (PSE) that includes the Doppler resolution as a sum over time as compared to a model with a complete closed form (Levin).

The quantitative performance is assessed with Monte Carlo simulations. The evaluation metric used in this article is the variance of the estimators. The Doppler frequencies in

the following examples are normalized $(\lambda/(2T) = 2V_a)$, where V_a is the unambiguous Doppler velocity of the radar. Therefore, the range of frequencies is from -0.5 to 0.5. In the following sections, "GT" refers to the ground truth. The normalized quantities are denoted with a subscript$_n$. The theoretical variances are denoted as "Theor" on the plots.

A. Parameter Estimation With $L = 1$

In this example, the simulated signal has parameters (also referred to as the ground truth) $\mu_{\text{fn}} = 2T\mu_v/\lambda = 0$ and $\sigma_{\text{fn}} = 2T\sigma_v/\lambda = 0.033$. The number of scatterers in the model is kept as $M = 10\,000$. The SNR input for the model (6) is 12 dB. The number of iterations used in the Monte Carlo simulation is 1024 for this analysis. The mean retrieval (using the Monte Carlo simulations) of the normalized mean Doppler frequency and the Doppler frequency width is shown in Fig. 1(a) and (b), respectively.
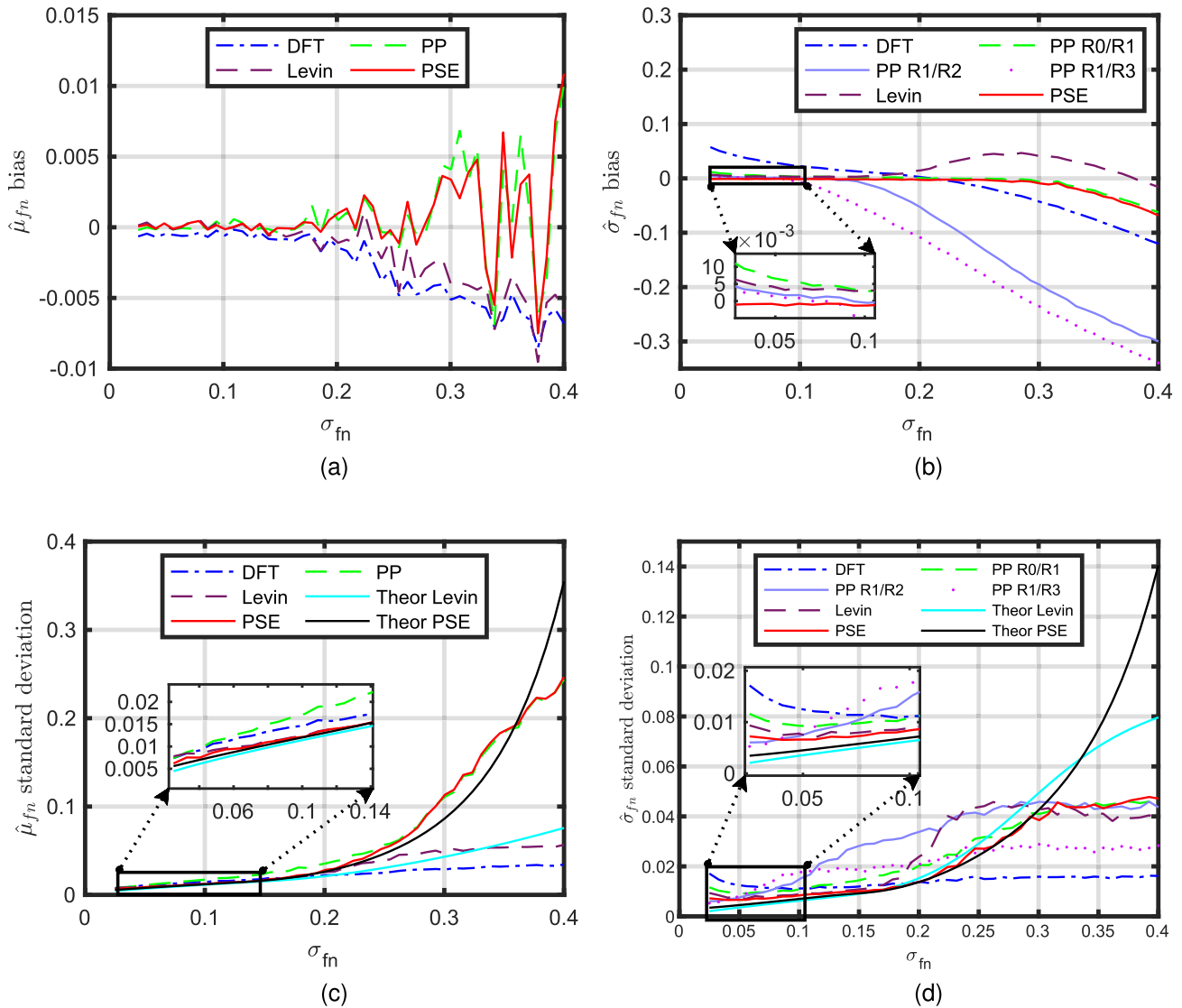
Fig. 2. Estimation and performance of the Doppler moments for $L = 1$ with respect to σ_{fn} at $\mu_{\text{fn}} = 0$: (a) biases in the estimates of the mean Doppler frequency normalized $\hat{\mu}_{fn}$; (b) Doppler frequency width normalized $\hat{\sigma}_{\text{fn}}$; (c) standard deviation in estimating the mean Doppler frequency normalized $\hat{\mu}_{\text{fn}}$; and (d) standard deviation in estimating the Doppler spectrum width normalized $\hat{\sigma}_{\text{fn}}$.

According to Fig. 1(a), all approaches perform similarly when the number of coherent samples is large for estimating the first moment. For a lower number of coherent samples (especially below $N = 30$), PSE and PP approaches have lower bias than the DFT and Levin's ML approaches. From Fig. 1(b), it can also be observed that the biases of the higher lag versions of PP PP R2/R1 and PP R3/R1 are lower than PP R0/R1, because the spectrum width considered for this example is relatively narrow. According to Fig. 1(b), PSE achieves convergence at a lower number of coherent samples (at $N > 30$) than the other approaches. The bias is -0.004, and percentage error is 13.34% at $N = 30$ for σ_{fn}. The variances of the estimates in μ_{fn} and σ_{fn} are computed numerically as a function of the number of coherent samples (N). The standard deviation is plotted in Fig. 1(c) and (d) for μ_{fn} and σ_{fn}, respectively. The standard deviations of the approaches are plotted for $N > 30$, which is the reciprocal of the true normalized frequency spectrum width ($1/\sigma_{\text{fn}}$). The minimum

number of coherent samples for the performance analysis is greater than $1/\sigma_{\text{fn}}$ (the normalized frequency resolution Δf_{fn} should be $0 < \Delta f_{\text{fn}} < 1/[\sigma_{\text{fn}}^{-1} - 1]$) to have sufficient resolution for the PSD and a low bias in the estimates.

According to Fig. 1(c) and (d), the variance of the PSE goes lower than the other techniques with an increase in the number of samples.

Performance is also evaluated as a function of the normalized Doppler spectrum width σ_{fn}, with a fixed normalized mean Doppler frequency ($\mu_{fn} = 0$) and a fixed number of coherent samples ($N = 64$). The biases in the estimation results are shown in Fig. 2(a) and (b) for the mean Doppler frequency and Doppler spectrum width, respectively. The performance analyses of both parameters are shown in Fig. 2(c) and (d) with the other approaches.

All the approaches perform similarly for the mean Doppler velocity $\sigma_{fn} = 0.2$. The PP and PSE approaches have large biases and oscillate around the true normalized mean Doppler.
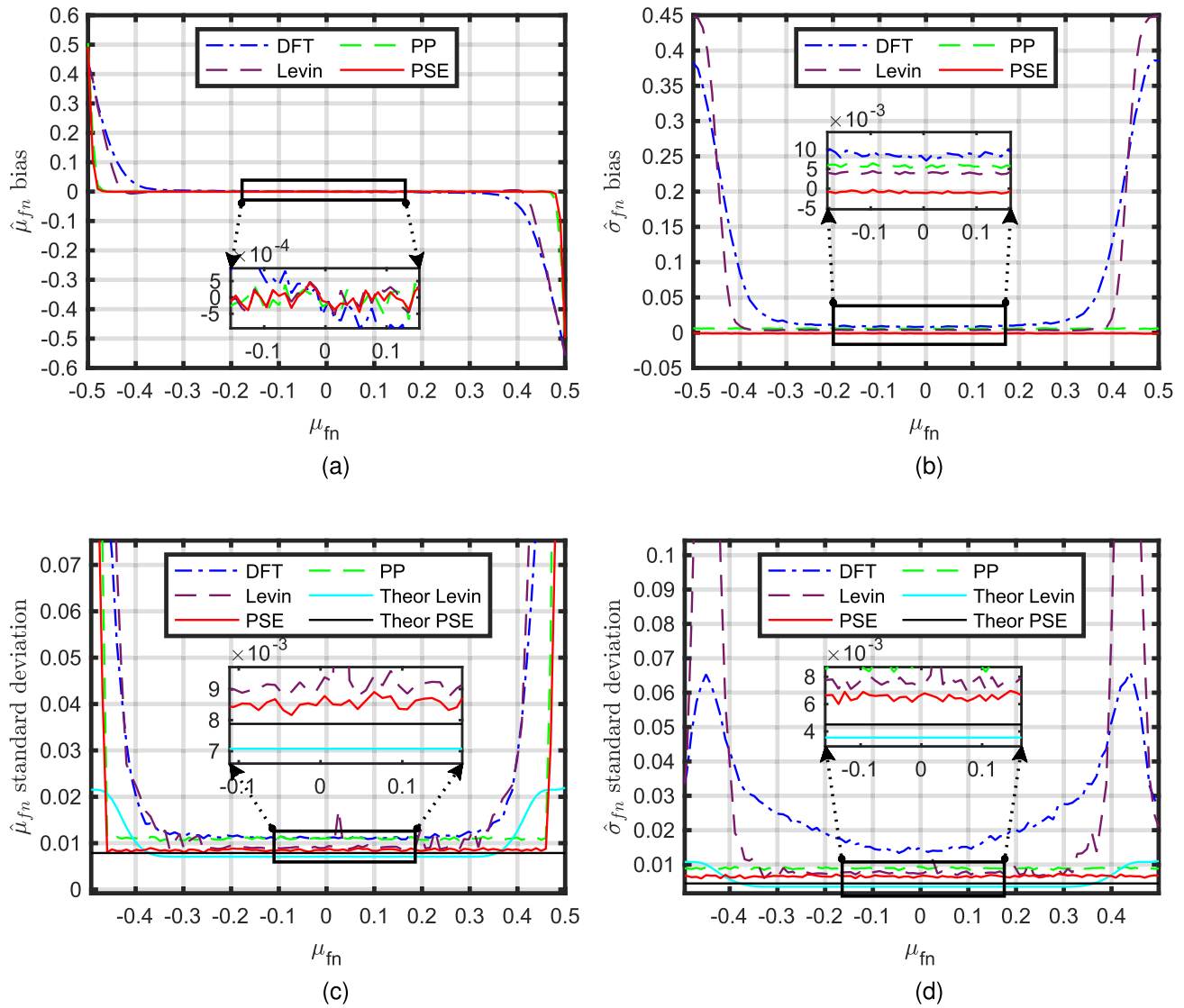
Fig. 3.   Estimation and performance of the Doppler moments for $L = 1$ with respect to μ_f at $\sigma_f = 0.05$: (a) biases in the estimates of the mean Doppler frequency normalized $\hat{\mu}_{fn}$; (b) Doppler frequency width normalized $\hat{\sigma}_{fn}$; (c) standard deviation in estimating the mean Doppler frequency normalized $\hat{\mu}_{fn}$; and (d) standard deviation in estimating the Doppler spectrum width normalized $\hat{\sigma}_{fn}$.

The variance of the PSE approach is lower as compared to the other approaches for the mean Doppler till $\sigma_{fn} < 0.2$. The DFT and Levin's approach have an increasing negative bias with increasing spectral width for $\sigma_{fn} > 0.2$.

It can be observed that the different versions of the PP approach give lower bias than the PSE approach for specific intervals of the spectrum width. It is well known from the literature that the PP approaches with larger lags give lower bias for smaller spectral widths and vice versa [25], [26]. However, to construct an adaptive lag estimator, some prior information has to be known for the spectral width such that one of the PP versions can be chosen. It is evident from Fig. 2(b) that the PSE approach performs adequately across all ranges of spectral widths. The bias increases for very large spectral widths $\sigma_{fn} > 0.25$.

For very low spectral widths $\sigma_{fn} < 0.04$, the PP versions R2/R1 and R3/R1 perform better and have lower variances than the PSE. For spectrum widths, $0.04 < \sigma_{fn} < 0.25$, PSE

has the lowest variance among all the approaches. For higher spectrum widths, PP R1/R0 and PSE approaches give similar variances. The PP R3/R1 and DFT show very low variances at very high spectrum widths $\sigma_{fn} > 0.25$ due to their significant biases.

The performance is further evaluated as a function of the normalized mean Doppler frequency μ_{fn} with a fixed normalized Doppler spectrum width ($\sigma_{fn} = 0.05$) and a fixed number of coherent samples ($N = 64$). The biases in the estimation results are shown in Fig. 3(a) and (b) for the mean Doppler frequency and Doppler spectrum width, respectively. The performance analyses of both parameters are shown in Fig. 3(c) and (d). The estimated mean Doppler frequency suffers from the aliasing near the unambiguous limit for all methods. The aliasing effect is observed at a lower mean Doppler frequency for the positive frequencies and higher mean Doppler frequency for the negative frequencies with the DFT and Levin's ML approaches than the PP and

PSE. The Doppler spectrum width estimated with PP and PSE approaches is not affected by the aliasing, whereas the other approaches suffer from the aliasing effect. The bias and variance of PSE are superior to the other approaches for the Doppler spectrum width estimate.

B. Performance Analysis With Respect to L

The performance analysis of PSE has been compared with Levin's ML approach with a different number of observations L, keeping the number of coherent samples constant $N = 64$. The performances are shown in Fig. 4(a) and (b). It can be observed that with an increase in L, the variance decreases and converges for both techniques. The variance of PSE is lower than Levin's ML approach.

C. Discussion on the Simulation Results

The following conclusions can be made from the performance analysis of the proposed estimator in the previous sub-sections. The minimum observation time duration required for an accurate estimation of the Doppler spectrum width for PSE is inversely proportional to the true velocity dispersion of the scatterers (for normalized spectrum widths of $\sigma_{fn} < 0.2$). For example, for a velocity dispersion of one-fortieth of the unambiguous velocity interval ($2V_a$) in one resolution cell ($\sigma_v = 2V_a/40$), the number of slow time samples needed with PSE should be at least more than 40 (or, the Doppler resolution of $\Delta v < 2V_a/39$) to measure the Doppler spectrum width accurately. The minimum number of slow-time samples per resolution cell can be used to decide the scanning rate of the radar in azimuth. For the case mentioned above, if one uses 64 samples at least for one resolution cell with 813.2 μs pulse repetition time, the radar needs to spend only 26 ms per resolution cell in azimuth. Suppose the azimuthal resolution cell is 2.5°; the scanning speed of the radar can be fixed to 16 rpm. If the rain is turbulent with velocity dispersion of ($\sigma_v = 2V_a/10$), and if we want to use only 15 samples in one resolution cell, we can set the scanning rate to 68 rpm with the configuration mentioned above.

As the model and algorithm explained in this article are developed to solve the estimation of Doppler moments considering the Doppler resolution, we do not specify a practical accuracy needed for such weather conditions. Based on the analysis of the bias of the PSE, necessary scan strategies can be applied for the required accuracy demanded by the applications.

As PSE uses a maximum likelihood technique performed numerically with an optimization algorithm (L-BFGS), it is challenging to provide a quantitative idea about the computational cost, unlike the nonparametric approaches. However, PSE has a lower computational cost than the ACV-based parametric approaches as it does not involve any matrix inverse operation.

VII. APPLICATION TO REAL DATA

The proposed approach has been applied to real radar data recorded from the MESEWI radar at the Delft University of
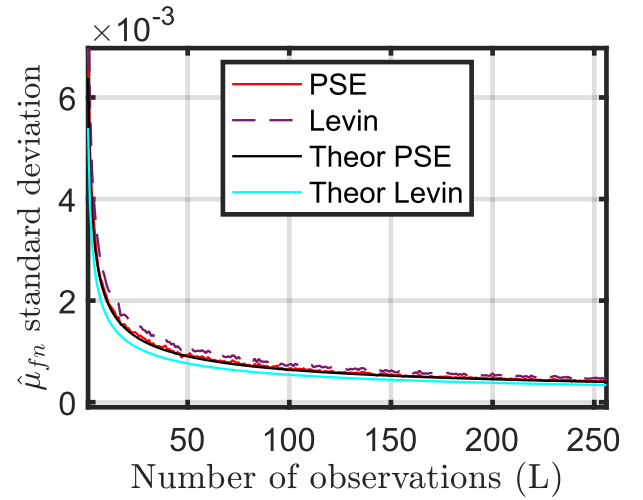
(a)
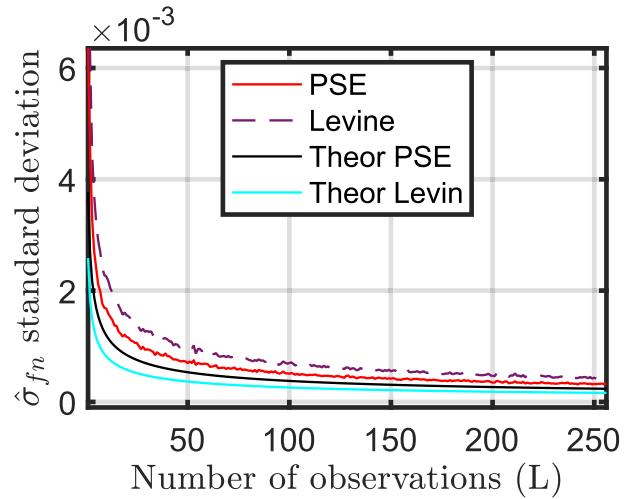
(b)

Fig. 4. Estimation and performance of the Doppler moments for $N = 64$ with respect to L. $\mu_{fn} = 0$ and $\sigma_{fn} = 0.033$ (a) Standard deviation in estimating the Mean Doppler Frequency normalized $\hat{\mu}_{fn}$. (b) Standard deviation in estimating the Doppler Spectrum Width normalized $\hat{\sigma}_{fn}$.

TABLE I

MESEWI RADAR SPECIFICATIONS

Parameter	Value
Center Frequency (f_c) (Hz)	9.4×10^9
PRI (T)	$813.2 \mu s$
Beamwidth in Azimuth ($d\phi$)	$2.5°$
Elevation Angle (ψ)	$30°$
ADC Sampling f_s (Hz)	4.92×10^6

Technology in the Netherlands. In these experiments, we have only used the signals from the HH channel. The MESEWI radar system is a fully polarimetric X-band (9.4 GHz) FMCW radar system. The PRI for each polarization is 406.6 μs. For one polarization, the PRI is 813.2 μs resulting in an maximal unambiguous Doppler velocity of $V_a = (\lambda)/(4 \times \text{PRT}) = 9.8$ m/s (λ is the central wavelength of the radar). The radar specifications are shown in Table I. The raw radar data are stored in a 3-D format with fast time, slow time, and azimuthal
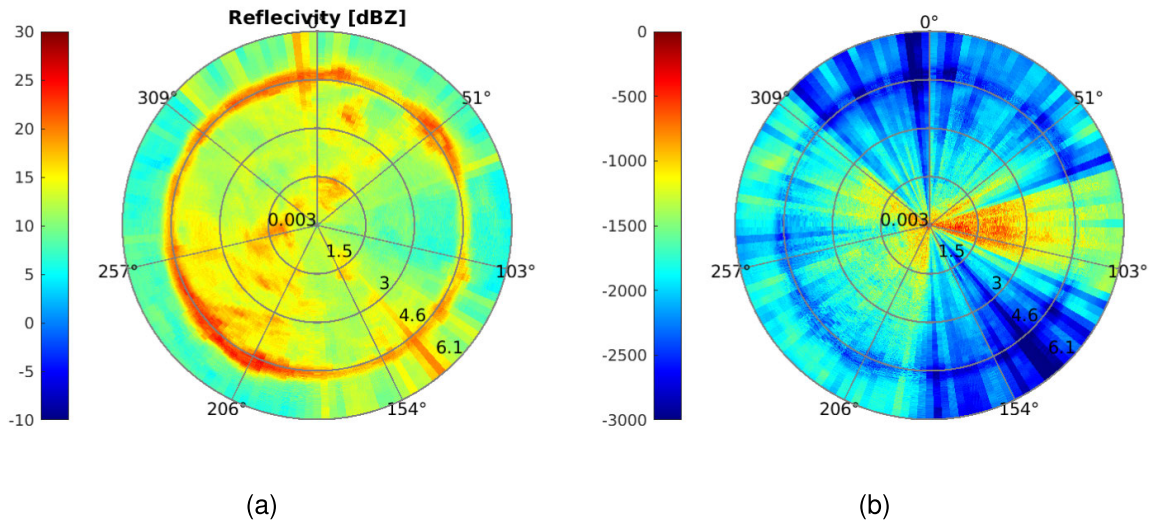
Fig. 5. (a) PPI plot of reflectivity using the DFT approach. (b) Log-likelihood (14) of PSE.

angles as the three dimensions. The data discussed below was collected when the radar was pointed to a fixed elevation angle of 30°. Two experiments were performed with an interval of 26 minutes (the second experiment was performed 26 min after completing the first). In the first experiment, the azimuthal rotation speed was one rotation per minute (1 rpm), while in the second one, it was five rotations per minute (5 rpm). The date of observation was 9 May 2023. It was a rainy day surrounding the area of Delft, Netherlands, which allowed us to observe clouds, the melting layer, and rain.

The preprocessing of sampled intermediate frequency data was performed along the following steps. After DC compensation, an FFT is applied on the fast time domain to ascertain the range dependence as it is an FMCW radar system. The mean is subtracted from each slow time sequence to remove the effects of the clutter. The Doppler processing is carried out on the slow time sequence for each range-azimuth resolution cell of the radar.

A. Experiment 1: Slow Scan of One Rotation per Minute

The bandwidth of operation is BW = 50 MHz for this experiment. The maximum range of the radar in this operational mode is 6 km $R_{max} = (f_s \times c)/(4BW \times PRF) = 6$ km (c is the speed of the electromagnetic wave), while the range resolution is three meters ($\Delta R = c/(2 \times BW) = 3$ m). After the range processing across the fast time, we have 512 echo samples for Doppler processing for each range-azimuth cell. For the DFT approach, several cells around the zero Doppler are chosen as the clutter region and are interpolated with a chosen noise level. The noise spectrum level (σ_n^2) is decided by taking the 15th percentile of the data contained in the PSD for each range-azimuth resolution cell because it is safe to assume that 15% of the data in the PSD are not from hydrometeors. The clutter region is not part of the observations for the PSE and Levin's ML approaches. The power scaling factor is determined from (11) for both Levin's ML approach and PSE. With the DFT approach, the total power estimate

(reflectivity) of the Doppler spectrum in each resolution cell is shown in Fig. 5(a). The reflectivity is shown here to explain some aspects of the mean Doppler and Doppler spectrum width estimated later in this article.

Fig. 5(a) shows a bright band ring of strong reflection around a range of 4 km. It could be attributed to the melting layer in the atmosphere where the precipitation forms [44]. The azimuth is considered clockwise (0° is toward the north) in this figure and the successive figures in this article. It can be observed that the reflectivity is considerably higher in ranges below 4 km, which corresponds to reflections from rain and in almost all azimuth sectors.

For the plan position indicator (PPI) plots for the mean Doppler and Doppler spectrum width, the 512 echo samples are separated into eight observations ($L = 8$), with each observation containing 64 coherent samples ($N = 64$) for the PSE and Levin's ML approach. The mean Doppler velocity and the spectrum width estimated with all the approaches considered in this article are shown in Fig. 6.

It is observed from the first row of Fig. 6 that the mean Doppler velocity estimates from all the approaches look similar except for some regions. The differences can be observed in the case of the DFT and Levin's ML approaches toward the edges of the figures (at more considerable distances from the radar). Although these approaches show near zero mean Doppler velocity, the PP and PSE approaches show a large deviation from zero. It is because the Doppler spectrum is nearly flat (having almost the same power in all velocity bins). Although the spectrum is nearly flat due to minor asymmetry around the zero Doppler, the other approaches are sensitive and estimate the mean Doppler velocity on either side of the zero Doppler. The existing literature [22], [38] shows that the PP approach is an unbiased estimator of the mean Doppler velocity and very robust at low signal-to-noise ratios. According to the results of the mean Doppler velocity, it is observed that the estimate of the proposed approach (PSE) is very close to that of the PP. In the directions around from 175° till 225° azimuth, there is aliasing of the mean Doppler
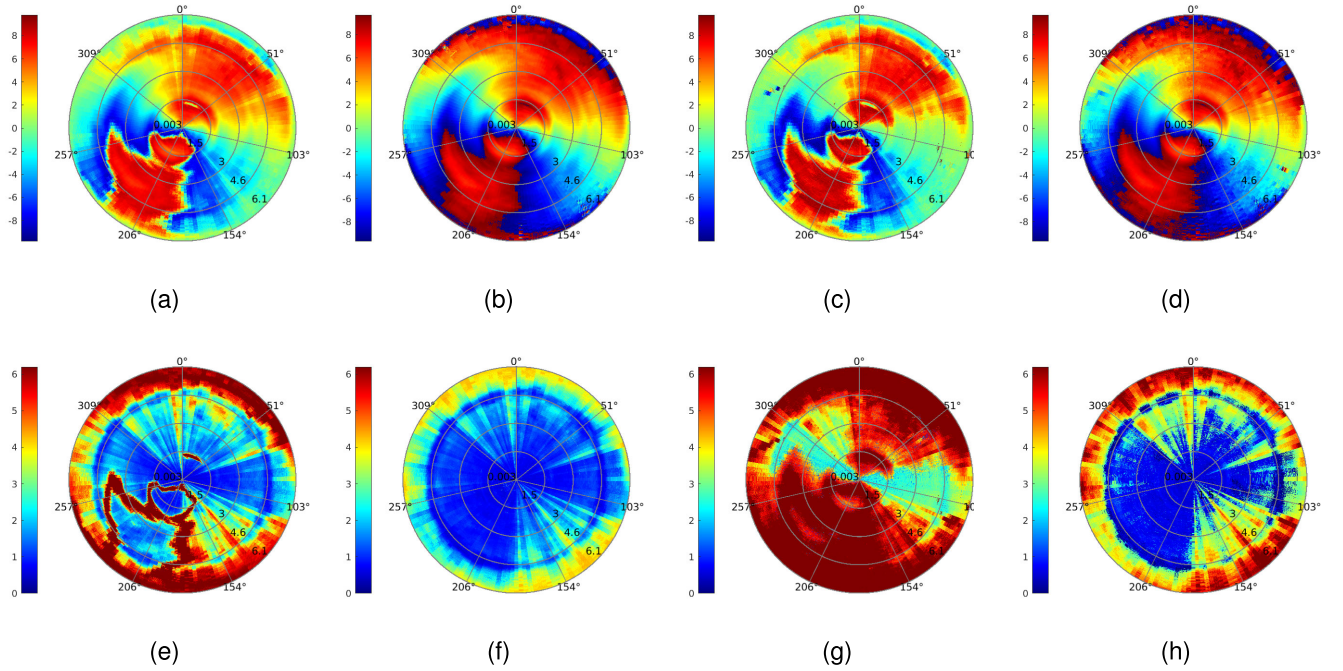
Fig. 6. PPI plots showing mean Doppler velocity and Doppler spectrum width with all the approaches discussed in this article. The first row shows the results of the mean Doppler velocity, and the second row shows the results of the Doppler spectrum width. (a) and (e) DFT, (b) and (f) PP, (c) and (g) Levin, and (d) and (h) PSE.

velocity. It has been captured by all the moment estimates. In the processing chain, it is logical first to perform de-aliasing based on the mean Doppler velocity and use an appropriate window of velocities to estimate the moments. However, we do not focus on the problem of de-aliasing the mean Doppler velocity in this article and focus more on the moment estimation only. Several observations are made based on the second row of Fig. 6. The borders of the aliased region are prominently visible on the Doppler spectrum width estimates of DFT and Levin's ML approaches having large values (till 9 m/s). This can be explained by the theoretical simulations in Section VI [Fig. 3(a) and (b)]. As the mean Doppler velocity approaches the unambiguous limit, the estimation of mean Doppler velocity becomes increasingly negatively biased. As the Doppler spectrum width is the square root of the second central moment and the DFT and Levin's ML approaches use PSD measurements, the spectrum width also becomes increasingly biased at the borders of this folded region. However, these high-spectrum width borders are not visible in the case of the PP and the PSE estimates because the PP estimator uses measurements in the time domain directly, and the PSE approach takes care of the aliasing (the semi-analytical model takes the finite observation window into account). A visual inspection of the mean Doppler velocity estimate suggests that the wind direction (the direction the precipitation field is moving) is toward $\phi = 15°$. The radial velocity observed by the radar is a scalar sum of projections of the horizontal wind (V) speed and the vertical speed (W) of the raindrops in the radial direction and is given by

$$\mu_v = V \cos \psi \cos(\phi - \phi_{\text{wind}}) + W \sin \psi \tag{16}$$
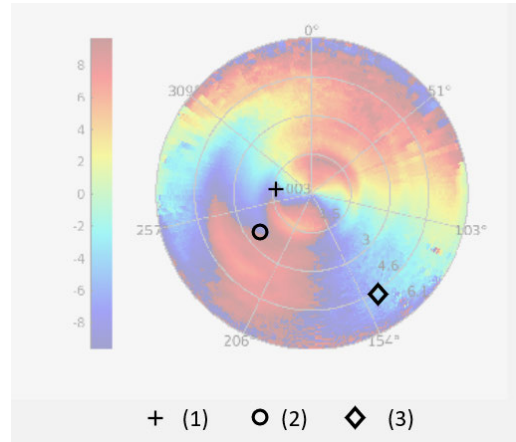
Fig. 7. PSE-derived mean Doppler velocity. The Doppler spectrum is analyzed in the highlighted areas of this figure.

where the ψ is the elevation angle from the ground, and ϕ_{wind} is the horizontal wind direction in azimuth. The vertical velocity W is usually associated with the reflectivity [45], [46] [47]. That is why the Mean Doppler velocity estimates are closer to zero toward $\phi = 135°$, and $\phi = 315°$ because these directions are perpendicular to the wind direction ($\phi - \phi_{\text{wind}} \approx 90°$).

In all the approaches discussed in this article, it has been assumed that the echo samples in the slow time domain are stationary and the spectrum is Gaussian shaped. Therefore, it is important to study not only the estimation performance but also the profile of the log-likelihood (14) as a function of the space because it gives a quantitative understanding of how well the real data fit the semi-parametric model discussed
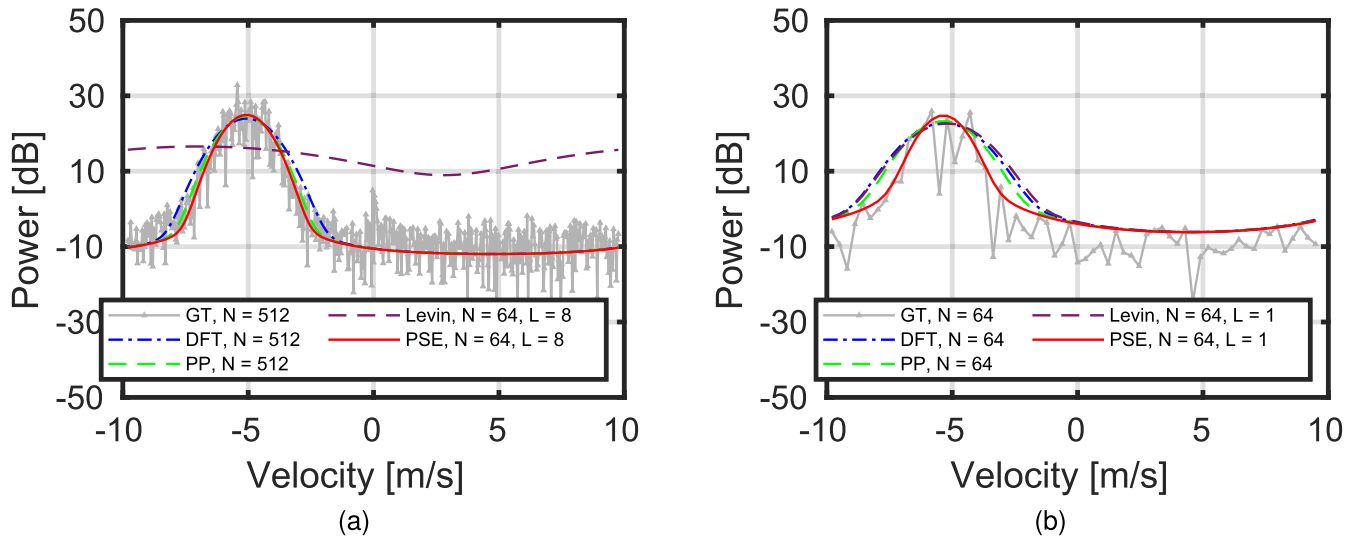
Fig. 8. Doppler spectrum reconstruction at cell (1): (a) 512 total samples and (b) 64 total samples.
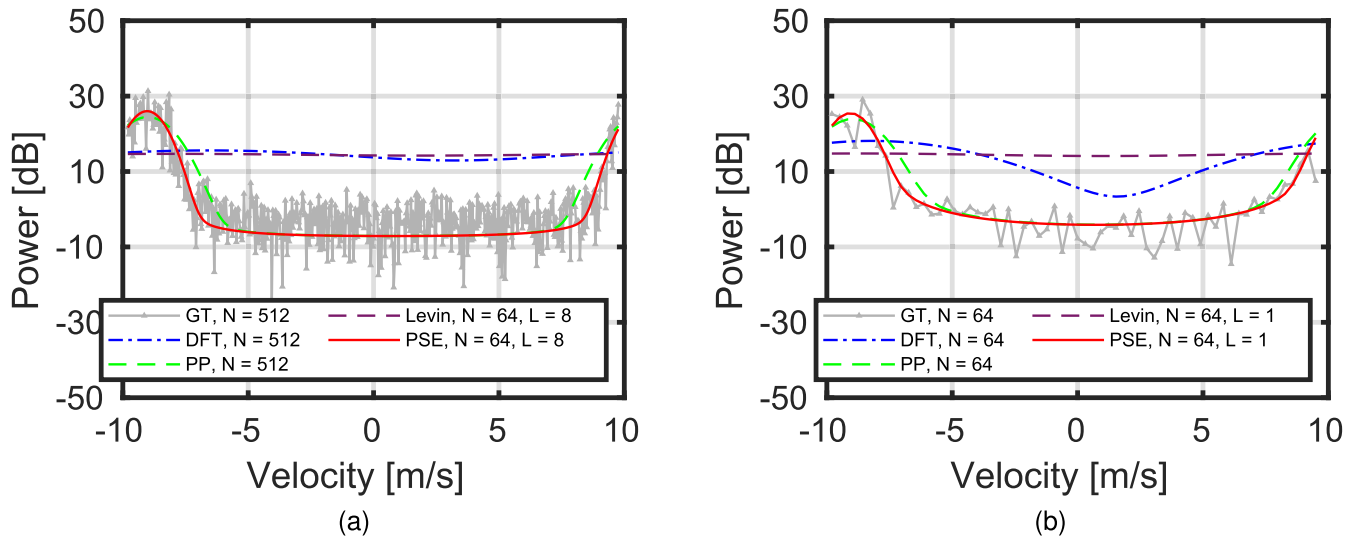
Fig. 9. Doppler spectrum reconstruction at cell (2): (a) 512 total samples and (b) 64 total samples.

in this article. The log-likelihood (14) has been plotted and shown in Fig. 5(b) to access the performance of the PSE approach on the real radar data. It can be observed that at high reflectivity regions below the melting layer shown in Fig. 5(a), the likelihood is larger than in the melting layer. It can be concluded that the model considered in the PSE approach fits the observations better in the case of the rain Doppler spectrum than in the melting layer.

The Doppler spectrum reconstruction is performed on specific resolution cells using all the approaches discussed in this article to validate the abovementioned test cases. The PSD of the echo samples is used as a reference (Ground Truth). The reconstruction is performed using the theoretical expected PSD of (10). Their estimated counterparts replace the parameters μ_v and σ_v in (10). To highlight the range-azimuth cells discussed in Sections VII-A1–A3, Fig. 6(d) is shown again in Fig. 7. Table II shows the coordinates of the chosen resolution cells for the analysis.

TABLE II
HIGHLIGHTED RESOLUTION CELLS' COORDINATES

Cell Number	R(km)	ϕ °
(1)	1.26	277
(2)	2.39	234
(3)	4.7	166

1) High Reflectivity Region (Precipitation Region): Fig. 8(a) shows the Doppler spectrum at the cell (1). The Doppler spectrum reconstruction for the same resolution cell is shown in Fig. 8(b) for $N = 64$ and $L = 1$ case. According to Fig. 8(b), it is observed that with only one observation $L = 1$ of 64 coherent samples, the PSE approach converges and reconstructs the spectrum better than the other approaches. The other approaches overestimate the Doppler spectrum width. This shows the superiority of the PSE approach with a low number of samples over the other approaches discussed in this article.
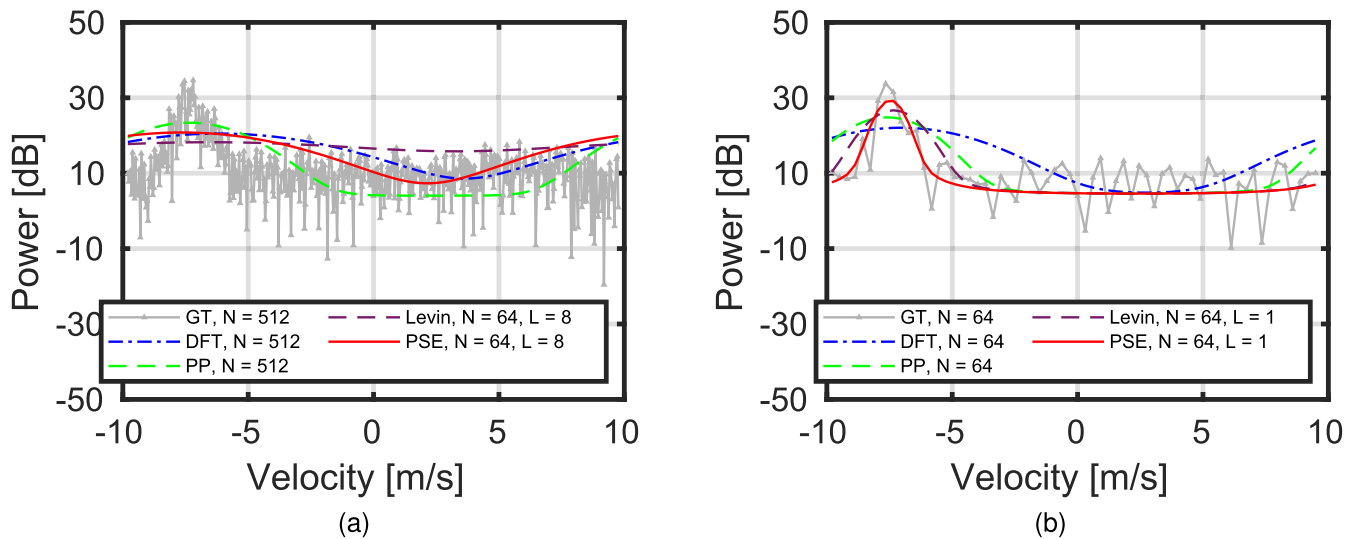
Fig. 10. Doppler spectrum reconstruction at cell (3): (a) 512 total samples (b) 64 total samples.
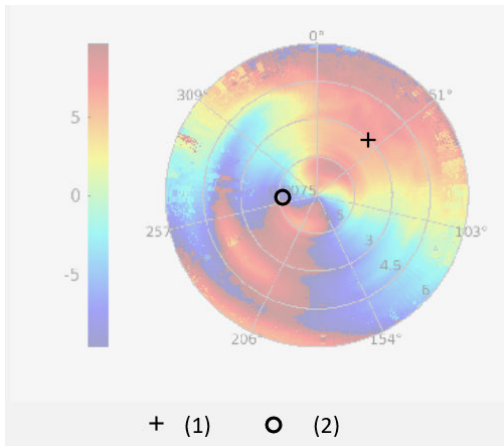
Fig. 11. PSE-derived mean doppler velocity. The Doppler spectrum is analyzed in the highlighted areas of this figure.

2) High Reflectivity Region With Doppler Aliasing:
Fig. 9(a) shows the Doppler spectrum at cell (2). The Doppler spectrum reconstruction for the same resolution cell is shown in Fig. 9(b) for $N = 64$ and $L = 1$ case. It is observed from Fig. 9(b) that the PSE approach converges only with one observation $L = 1$ of 64 coherent samples. In addition to that, the results of Fig. 9(a) and (b) validate the theoretical conclusions made on Fig. 3(b). The PP and PSE approaches are immune to the Doppler aliasing in the Doppler spectrum width estimate case. On the other hand, the other approaches overestimate the Doppler spectrum width.

3) Melting Layer Region (Low PSE Likelihood Region):
Fig. 10(a) shows the Doppler spectrum at the cell (3). The Doppler spectrum reconstruction for the same resolution cell is shown in Fig. 10(b) for $N = 64$ and $L = 1$ case. According to Fig. 10(a), all moment estimators cannot reconstruct the spectrum with a large number of samples. The Gaussian spectrum shape assumption is violated for a long record of samples at the melting layer. It is confirmed by lower log-likelihood (14) values at the melting layer compared to the precipitation

area, as shown in Fig. 5(b). The log-likelihood (14) at this range-resolution cell for $N = 64$, and $L = 8$ is -2891. However, according to Fig. 10(b), PSE fitting is superior to the other approaches when a short record of only 64 echo samples is used. The log-likelihood (14) for $N = 64$, and $L = 1$ is -334. From this analysis, it can be concluded that the Doppler spectrum at the melting layer can only assume stationarity for a short period.

B. Application to Fast Scanning Radar Data

Under the assumption that the spectral content (in terms of the spectral width) of the echo signals received from the multiple scans (from the precipitation regions) remains unchanged over this period, the PSE has been applied to real data acquired from multiple scans of the MESEWI radar with a fast scan in azimuth. In this experiment (mentioned as the second measurement at the beginning of the section), the bandwidth of operation was 20 MHz, and consequently, the range resolution was $\Delta R = c/(2 \times \text{BW}) = 7.5$ m. The maximum range in this example was $R_{\max} = (f_s \times c)/(4\text{BW} \times \text{PRF}) = 15$ km. However, in all the PPI plots, the range is shown till 6 km to avoid the region above the melting layer. The number of echo samples was 100 per resolution cell per scan. The 100 echo samples were grouped into two 50 coherent samples. Five azimuthal scans are processed, resulting in ten PSD observations per resolution cell ($L = 10$). The real data discussed in this section were acquired on the same day as the data discussed in Section VII-A. As the data was acquired after 26 min of the first experiment, the spatial variability of reflection differs from the case shown in Fig. 6. The moment estimation uses both PSE and Levin's ML techniques. The performance is evaluated by reconstructing the spectrum with the moments derived similar to Section VII-A for a few resolution cells. The reconstruction is compared with the PSD of all the observations ($1 \leq L \leq 10$ in this case). The noise variance estimate here is determined only from the first scan of the radar. The resolution cells chosen for the analysis of the reconstruction are highlighted on top
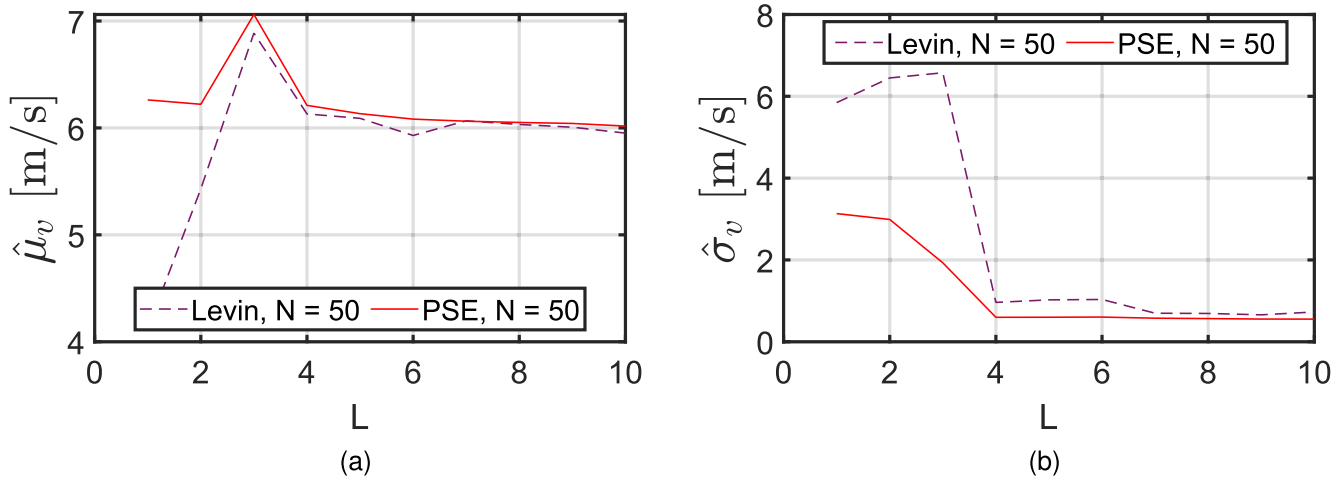
Fig. 12. Doppler moments estimation on real radar data with respect to number of observations L at resolution cell (1): (a) Mean Doppler velocity $\hat{\mu}_v$ m/s and (b) Doppler spectrum width $\hat{\sigma}_v$ m/s.
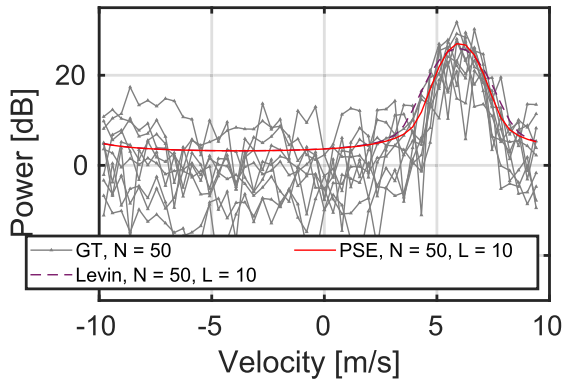
Fig. 13. Doppler spectrum reconstruction with $L = 10$. Incoherent processing of five scans of the radar at cell (1).

TABLE III
HIGHLIGHTED RESOLUTION CELLS' COORDINATES

Cell Number	R(km)	ϕ °
(1)	2.89	48
(2)	1.34	264

of the Fig. 11, which shows the PPI plot of the mean Doppler velocity retrieved from PSE after incoherently processing five scans of the radar data. Table III shows the coordinates of the chosen resolution cells for the analysis.

The estimation of the first and second Doppler moments are shown in Fig. 12(a) and (b) with respect to L at the resolution cell (1). It can be observed that both the PSE and Levin's ML approaches converge to the same estimates with an increasing number of scans, but the rate of convergence of PSE is better than that of Levin's ML approach. As the resolution cell is inside the precipitation region, the approximation of the PSD with a Gaussian spectrum is adequate. The spectrum reconstruction with PSE and Levin is shown in Fig. 13 at $L = 10$. In the resolution cell (2), the mean Doppler velocity exceeds the maximum unambiguous velocity and Doppler spectrum aliasing takes place. The estimation of the first and second Doppler moments for this situation are shown

in Fig. 14(a) and (b) with respect to L. It can be observed that the spectrum width estimate of the PSE approach is not affected by the aliasing of the Doppler spectrum, while Levin's ML approach gives completely wrong results. The spectrum reconstruction with both approaches is shown in Fig. 15 at $L = 10$. The PPI plots of the mean Doppler velocity and spectrum width are shown in Fig. 16 with five scans ($L = 10$) integrated into the estimation until the melting layer. It can be observed that the PSE approach is not affected by the Doppler aliasing when it comes to estimating the Doppler spectrum width.

VIII. CONCLUSION

This article proposes a maximum likelihood approach (PSE) to estimate Doppler spectral moments with a few coherent echo samples for weather-like targets such as precipitation. The proposed parametric model for the Doppler power spectrum is a function of the observation time duration and the precipitation targets' velocity parameters. For a continuous Gaussian spectrum, a semi-analytical form of the PSD has been derived in this article. The estimator's performance is studied with respect to the number of coherent Doppler samples using computer-simulated radar echo samples and compared with other existing estimators. It is shown that the performance of the PSE (with a low number of coherent samples) is superior to the existing classical methods, such as DFT and PP and Levin's ML approach for the Doppler spectrum width. The number of coherent samples required for accurately estimating the Doppler spectrum width using the PSE can be characterized by the true normalized Doppler frequency dispersion σ_{fn} as $N > 1/\sigma_{\text{fn}}$ (for $\sigma_{\text{fn}} < 0.2$). However, the classical techniques require much longer observation time than this because of a larger bias caused by finite Doppler resolution. An important application of this approach is realized in the case of a fast-scanning radar in azimuth. The advantage of PSE over the classical approaches like DFT and PP is that it can accommodate multiple measurements of the Doppler spectrum (referred to as L in this article) that are incoherent among themselves (each of the PSDs contains
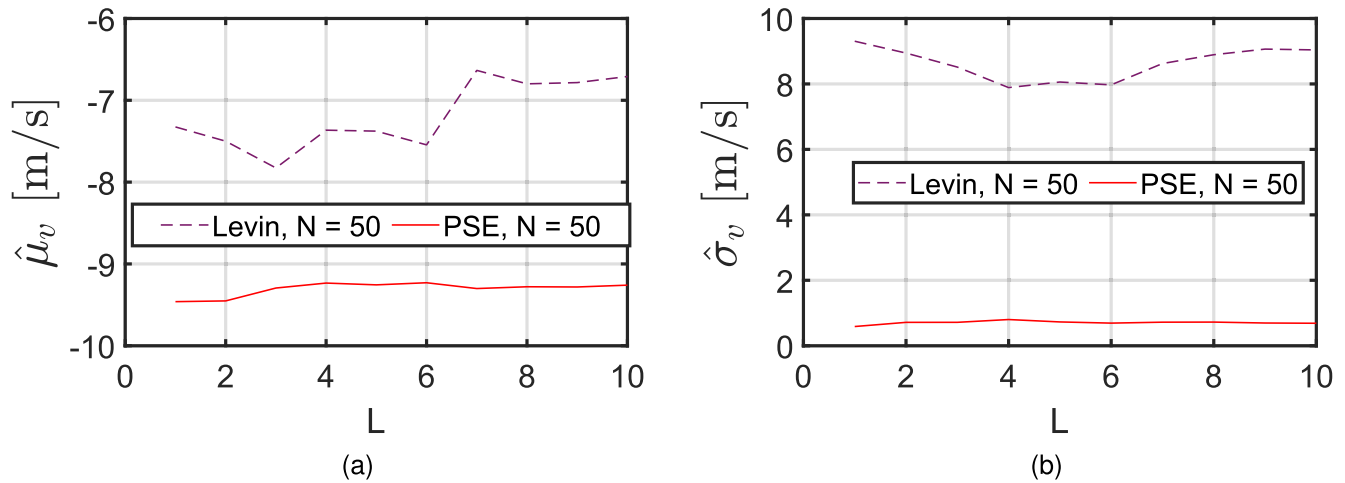
Fig. 14. Doppler moments estimation on real radar data with respect to the number of observations L at resolution cell (2): (a) Mean Doppler velocity μ_v m/s and (b) Doppler spectrum width σ_v m/s.
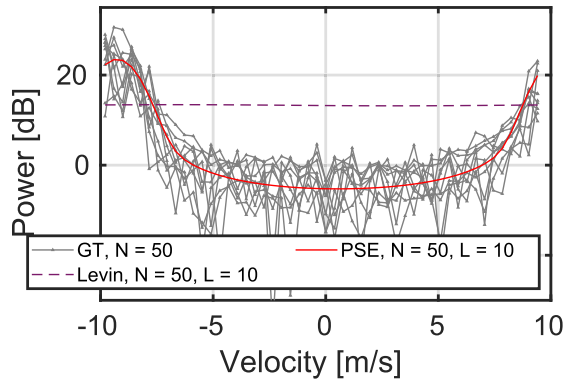
Fig. 15. Doppler spectrum reconstruction with $L = 10$. Incoherent processing of five scans of the radar at cell (2).

N coherent echo samples). The performance analysis of the PSE has been carried out with the number of observations (L) at a fixed N, ($N > 1/\sigma_{\text{fn}}$) and compared with Levin's ML approach. It is concluded that the estimation accuracy increases with the number of observations L. The performance analysis includes a comparison of estimation variances of different approaches. The estimated parameter variance converges to the CRB when the sample size approaches infinite (Appendix B).

The PSE is applied to real radar observations collected from the MESEWI radar at TU Delft. For resolution volumes with rain having high reflectivity, it is shown that an accurate estimation of the parameters with PSE is achieved with a relatively small number of samples. In some resolution volumes, especially in the melting layer, the echo samples in time do not follow the assumption that the PSD is Gaussian and stationary for a long period. For these cases, the estimation of the Doppler moments is erroneous. However, using a short data record, the Doppler spectrum can be reconstructed accurately with the PSE approach. A comparison of the Doppler moments estimation using the techniques discussed in this article is shown for all range-azimuth radar cells. As the proposed approach performs superior for stationary Gaussian-like weather Doppler spectrum only, a more accurate parametric

model will be derived for a more generic weather-like Doppler spectrum with extra parameters such as skewness, clutter, and a variable number of spectral shapes (variable number of extended targets) in the future.

A similar approach also could be developed using a semi-analytical form of the ACV function of the time series instead of the PSD. However, the ACV-based maximum likelihood approaches usually involve an inverse ACV matrix, leading to unnecessary computational overload.

APPENDIX A
EXPECTED VALUE OF THE POWER SPECTRUM

The expectation of the square of the modulus of the spectrum function (taken from [9]) is presented in this Appendix. Here, for the derivation, we do not use the normalization $(1/N)$. A change of parametrization from velocity to angular frequency ($\omega = (4\pi T/\lambda)v$) is used in the derivation for mathematical simplicity

$$\mathbb{E}\left[\left|S(\omega)\right|^2\right] = A^2 \mathbb{E}\left[\sum_{m=1}^{M} \frac{\sin^2\left(N\frac{(\omega_{m,r}-\omega)}{2}\right)}{\sin^2\left(\frac{\omega_{m,r}-\omega}{2}\right)}\right]. \quad (17)$$

As the velocities of the raindrops are assumed i.i.d., the right-hand side of (17) can be approximated to the following integral:

$$\mathbb{E}\left[\left|S(\omega)\right|^2\right] = A^2 M \int_{-\infty}^{+\infty} \frac{\sin^2\left(N\frac{(x-\omega)}{2}\right)}{\sin^2\left(\frac{x-\omega}{2}\right)} p(x) dx \quad (18)$$

where the $p(x)$ is the probability density function of the frequencies which is assumed to be Gaussian in this case. The integral is then

$$\mathbb{E}\left[\left|S(\omega)\right|^2\right] = A^2 M \int_{-\infty}^{+\infty} \frac{\sin^2\left(N\frac{(x-\omega)}{2}\right)}{\sin^2\left(\frac{x-\omega}{2}\right)} \frac{1}{\sqrt{2\pi\sigma_\omega^2}}$$
$$\times \exp\left(-\frac{(x-\mu_\omega)^2}{2\sigma_\omega^2}\right) dx \quad (19)$$

where μ_ω and σ_ω are normalized angular frequency equivalents of the normalized Doppler frequencies. It can be further
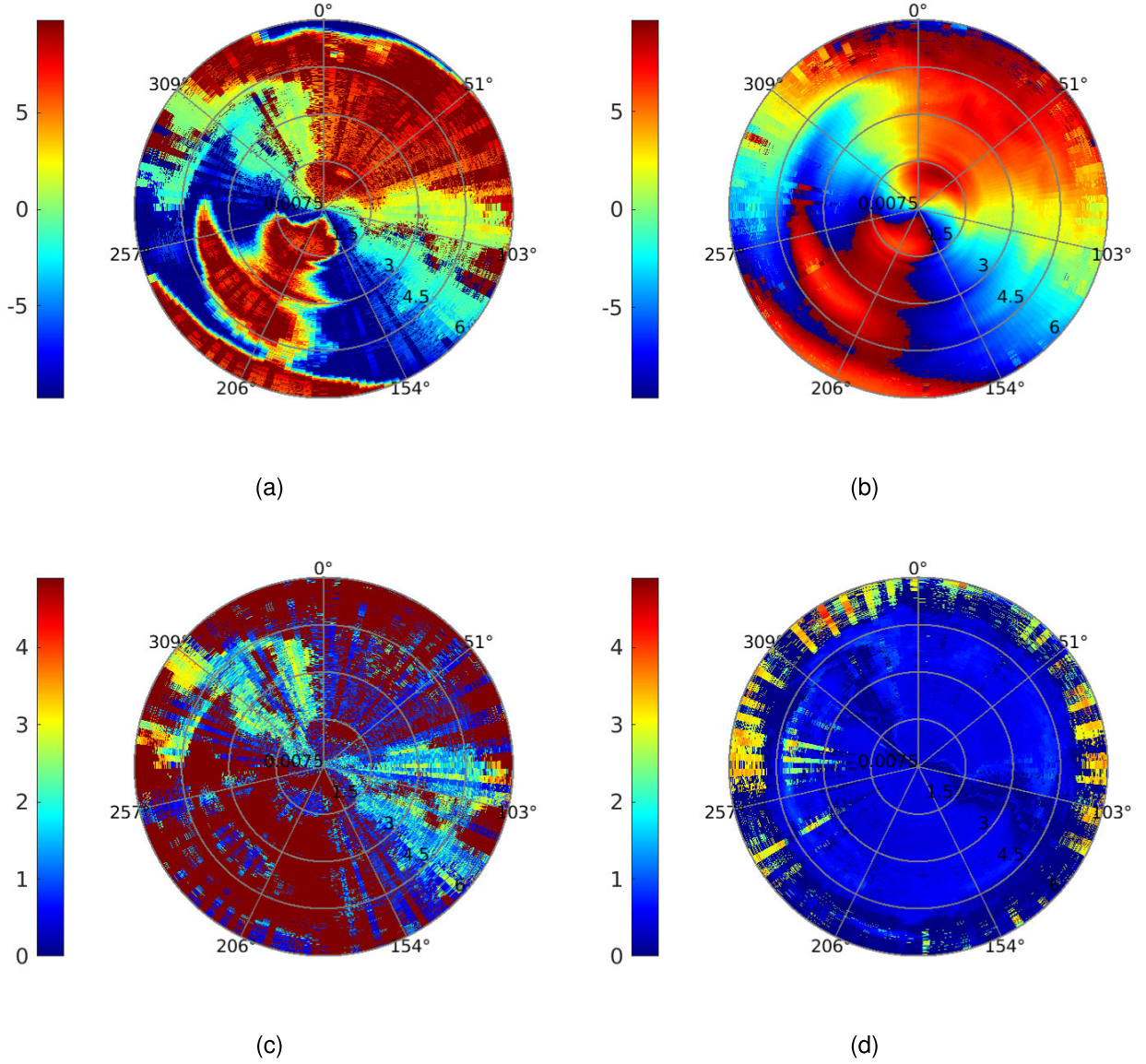
Fig. 16. PPI plots at $L = 10$. Incoherent processing of five scans of the radar: (a) mean Doppler velocity μ_v m/s with Levin's ML approach; (b) mean Doppler velocity μ_v m/s with PSE; (c) Doppler spectrum width σ_v m/s with Levin's ML approach, and (d) Doppler spectrum width σ_v m/s with PSE.

simplified as

$$
\mathbb{E}\left[\left|S(\omega)\right|^2\right] = A^2 M \int_{-\infty}^{+\infty} \exp(-j(N-1)(x-\omega))
$$
$$
\times \left(\frac{\exp(jN(x-\omega)) - 1}{\exp(j(x-\omega)) - 1}\right)^2 \frac{1}{\sqrt{2\pi\sigma_\omega^2}}
$$
$$
\times \exp\left(-\frac{(x-\mu_\omega)^2}{2\sigma_\omega^2}\right) dx. \tag{20}
$$

If a parametrization $\zeta = \exp(j(x-\omega))$ is applied, $\exp(-j(N-1)(x-\omega)) \times ((\exp(jN(x-\omega)) - 1 / \exp(j(x-\omega)) - 1))^2$ takes the following form:

$$
I(\zeta) = \zeta^{-(N-1)} \left(\frac{\zeta^N - 1}{\zeta - 1}\right)^2 \tag{21}
$$

where the expression $(\zeta^N - 1/\zeta - 1)$ is equal to a finite length (N term) sum of a geometric progression with starting point 1

and a common factor of ζ

$$
I(\zeta) = \zeta^{-(N-1)} \left(\sum_{n=0}^{N-1} \zeta^n\right)^2. \tag{22}
$$

The expression $(\sum_{n=0}^{N-1} \zeta^n)^2$ can be expanded using the principles of multinomial expansion, which then can be generalized by the following expression:

$$
I(\zeta) = N + \sum_{n=1}^{N-1} n\left(\zeta^{n-N} + \zeta^{N-n}\right). \tag{23}
$$

Replacing ζ as the function of x, we have

$$
I(x) = N + \sum_{n=1}^{N-1} n(\exp(j(x-\omega)(n-N))
$$
$$
+ \exp(j(x-\omega)(N-n))). \tag{24}
$$

This can be rewritten by a change in parametrization $n = N-q$

$$
I(x) = N + \sum_{q=1}^{N-1} (N - q)(\exp(j(x - \omega)q)
$$

$$
+ \exp(-j(x - \omega)q)). \quad (25)
$$

Hence, the original integral (17) can be written as follows:

$$
\mathbb{E}\left[|S(\omega)|^2\right]
$$

$$
= A^2 M \int_{-\infty}^{+\infty} \frac{1}{\sqrt{2\pi\sigma_\omega^2}} \exp\left(-\frac{(x - \mu_\omega)^2}{2\sigma_\omega^2}\right) I(x)dx. \quad (26)
$$

The integral of a complex exponential function multiplied with a Gaussian function is generalized by the following relation:

$$
\int_{-\infty}^{+\infty} \frac{1}{\sqrt{2\pi\sigma^2}} \exp\left(-\frac{(x - \mu)^2}{2\sigma^2}\right) \exp(j\eta x)dx
$$

$$
= \exp\left(-\frac{\sigma^2\eta^2}{2}\right) \exp(j\eta\mu). \quad (27)
$$

Using (27), we can rewrite (26) as follows:

$$
\mathbb{E}\left[|S(\omega)|^2\right]
$$

$$
= A^2 M \left(N + \sum_{q=1}^{N-1} (N-q) \times \left[\exp\left(-\frac{\sigma_\omega^2 q^2}{2}\right) \times (\exp(jq(\mu_\omega - \omega))\right.\right.
$$

$$
\left.\left. + \exp(-jq(\mu_\omega - \omega)))\right]\right) \quad (28)
$$

which then simplifies to

$$
\mathbb{E}\left[|S(\omega)|^2\right] = A^2 M \left(N + 2\sum_{q=1}^{N-1} (N - q)\right.
$$

$$
\left. \times \left[\exp\left(-\frac{\sigma_\omega^2 q^2}{2}\right) \times \cos(q(\mu_\omega - \omega))\right]\right). \quad (29)
$$

Changing the parametrization from angular frequency to velocity, and normalizing it with the number of samples N, we have the following final expression for the PSD:

$$
\mathbb{E}\left[\frac{1}{N}|S(v)|^2\right]
$$

$$
= A^2 M \left(1 + 2\sum_{q=1}^{N-1} \left(1 - \frac{q}{N}\right) \times \left[\exp\left(-\left(\frac{4\pi T}{\lambda}\right)^2 \frac{\sigma_v^2 q^2}{2}\right)\right.\right.
$$

$$
\left.\left. \times \cos\left(\frac{4\pi T}{\lambda} q(\mu_v - v)\right)\right]\right). \quad (30)
$$

APPENDIX B
THEORETICAL VARIANCE AND THE CRAMER RAO LOWER BOUND OF PSE

The log-likelihood of (14) is used to compute the theoretical variance. Here, as there are two parameters (here we consider the normalized frequency parameters) $\Theta = [\theta_a, \theta_b] = [\mu_v, \sigma_v]$, the Fisher matrix is of dimension (2×2). The entries of the Fisher matrix are given by

$$
I_{a,b} = -\mathbb{E}\left[\frac{\partial^2 \log\left(p(\mathbf{Z}|\Theta)\right)}{\partial\theta_a \partial\theta_b}\right]. \quad (31)
$$

The derivative of (14) with respect to any one of the parameters (θ_a or θ_b) is given by

$$
\frac{\partial \log\left(p(\mathbf{Z}|\Theta)\right)}{\partial\theta_a} = -\sum_{i=1}^{N}\left[\frac{L}{F(v_i, \Theta) + \sigma_n^2}\frac{\partial F(v_i, \Theta)}{\partial\theta_a}\right.
$$

$$
\left. - \frac{\sum_{l=1}^{L} Z_l(v_i)}{\left(F(v_i, \Theta) + \sigma_n^2\right)^2}\frac{\partial F(v_i, \Theta)}{\partial\theta_a}\right]. \quad (32)
$$

The derivative of the above expression with respect to the other parameter (θ_a or θ_b) is therefore given by (Using only F instead of $F(v_i, \Theta)$ and Z_l instead of $Z_l(v_i)$ for convenience)

$$
\frac{\partial^2 \log\left(p(\mathbf{Z}|\Theta)\right)}{\partial\theta_a\theta_b}
$$

$$
= -\sum_{i=1}^{N}\left[\frac{-L\left(F + \sigma_n^2\right) + 2\sum_{l=1}^{L} Z_l}{\left(F(v_i, \Theta) + \sigma_n^2\right)^3}\left(\frac{\partial F}{\partial\theta_a}\right)\left(\frac{\partial F}{\partial\theta_b}\right)\right.
$$

$$
\left. + \frac{L\left(F + \sigma_n^2\right) - \sum_{l=1}^{L} Z_l}{\left(F(v_i, \Theta) + \sigma_n^2\right)^2}\frac{\partial^2 F}{\partial\theta_a\partial\theta_b}\right]. \quad (33)
$$

The expectation of the expression above is given by (using the fact that $\mathbb{E}[Z] = F + \sigma_n^2$)

$$
\mathbb{E}\left[\frac{\partial^2 \log\left(p(\mathbf{Z}|\Theta)\right)}{\partial\theta_a\theta_b}\right]
$$

$$
= -\sum_{i=1}^{N}\left[\frac{L}{\left(F(v_i, \Theta) + \sigma_n^2\right)^2}\left(\frac{\partial F}{\partial\theta_a}\right)\left(\frac{\partial F}{\partial\theta_b}\right)\right]. \quad (34)
$$

For normalized velocity parameters ($\lambda/(2T) = 2V_a$), the function F can be written as follows:

$$
F(f, \mu_{\text{fn}}, \sigma_{\text{fn}})
$$

$$
= M \times \left[1 + 2 \cdot \sum_{q=1}^{N-1}\left(1 - \frac{q}{N}\right)\right.
$$

$$
\left. \times \exp\left(-2\pi^2\sigma_{\text{fn}}^2 q^2\right) \times \cos(2\pi q(\mu_{\text{fn}} - f))\right]. \quad (35)
$$

The derivatives of (35) are given in the following:

$$
\frac{\partial F}{\partial\mu_{\text{fn}}} = -4\pi \cdot M \cdot \sum_{q=1}^{N-1} q\left(1 - \frac{q}{N}\right)
$$

$$
\times \exp\left(-2\pi^2\sigma_{\text{fn}}^2 q^2\right) \sin(2\pi q(\mu_{\text{fn}} - f)). \quad (36)
$$

$$\frac{\partial F}{\partial \sigma_{\text{fn}}} = -8\pi^2 M \times \sum_{q=1}^{N-1} q^2 \left(1 - \frac{q}{N}\right) \exp\left(-2\pi^2 \sigma_{\text{fn}}^2 q^2\right)$$

$$\times \cos(2\pi q(\mu_{\text{fn}} - f)). \tag{37}$$

Therefore, the theoretical variance is given by

$$\mathbb{V}^{\text{Theor}}\left[\hat{\theta}_a\right] \geq \mathbf{I}_{a,a}^{-1}. \tag{38}$$

It is also known as the square of the reciprocal of the sensitivity [31, eq. (4)]. As the estimator is unbiased for both the parameters for $N \to \infty$, (38) can be used at $N \to \infty$ to compute the unbiased CRB

$$\mathbb{V}\left[\hat{\theta}_i\right] \geq \mathbf{I}_{a,a}^{-1}\big|_{N \to \infty}. \tag{39}$$

A closed form of the unbiased CRB is out of the scope of this article.

ACKNOWLEDGMENT

REFERENCES

[1] K. A. Browning and R. Wexler, "The determination of kinematic properties of a wind field using Doppler radar," *J. Appl. Meteorol.*, vol. 7, no. 1, pp. 105–113, Feb. 1968.

[2] C.-J. Qiu and Q. Xu, "A simple adjoint method of wind analysis for single-Doppler data," *J. Atmos. Ocean. Technol.*, vol. 9, no. 5, pp. 588–598, Oct. 1992.

[3] A. Shapiro, S. Ellis, and J. Shaw, "Single-Doppler velocity retrievals with Phoenix II data: Clear air and microburst wind retrievals in the planetary boundary layer," *J. Atmos. Sci.*, vol. 52, no. 9, pp. 1265–1287, May 1995.

[4] C.-J. Qiu and Q. Xu, "Least squares retrieval of microburst winds from single-Doppler radar data," *Monthly Weather Rev.*, vol. 124, no. 6, pp. 1132–1144, Jun. 1996.

[5] Y.-C. Liou, "An explanation of the wind speed underestimation obtained from a least squares type single-Doppler radar velocity retrieval method," *J. Appl. Meteorol.*, vol. 41, no. 7, pp. 811–823, Jul. 2002.

[6] C.-J. Qiu, A.-M. Shao, S. Liu, and Q. Xu, "A two-step variational method for three-dimensional wind retrieval from single Doppler radar," *Meteorol. Atmos. Phys.*, vol. 91, nos. 1–4, pp. 1–8, Jan. 2006.

[7] Y.-C. Liou, H. B. Bluestein, M. M. French, and Z. B. Wienhoff, "Single-Doppler velocity retrieval of the wind field in a tornadic supercell using mobile, phased-array, Doppler radar data," *J. Atmos. Ocean. Technol.*, vol. 35, no. 8, pp. 1649–1663, Aug. 2018.

[8] A. O. Nijhuis, "Radar remote sensing of wind vector and turbulence intensity fields from raindrop backscattering," Ph.D. dissertation, Dept. Microelectron., Delft Univ. Technol., Delft, The Netherlands, 2019.

[9] F. J. Yanovsky, H. W. J. Russchenberg, L. P. Ligthart, and Y. A. Aver'yanova, "Model of drop canting in microwave remote sensing of rain," in *Proc. 4th Int. Kharkov Symp. 'Phys. Eng. Millim. Sub-Millim. Waves'*, vol. 1, Jun. 2001, pp. 471–473.

[10] F. J. Yanovsky, I. G. Prokopenko, K. I. Prokopenko, H. W. J. Russchenberg, and L. P. Ligthart, "Radar estimation of turbulence eddy dissipation rate in rain," in *Proc. IEEE Int. Geosci. Remote Sens. Symp.*, vol. 1, Jun. 2002, pp. 63–65.

[11] F. J. Yanovsky, H. W. J. Russchenberg, and C. M. H. Unal, "Retrieval of information about turbulence in rain by using Doppler-polarimetric radar," *IEEE Trans. Microw. Theory Techn.*, vol. 53, no. 2, pp. 444–450, Feb. 2005.

[12] P. Borque, E. Luke, and P. Kollias, "On the unified estimation of turbulence eddy dissipation rate using Doppler cloud radars and LiDARs," *J. Geophys. Res., Atmos.*, vol. 121, no. 10, pp. 5972–5989, May 2016.

[13] B. E. Sheppard, "Measurement of raindrop size distributions using a small Doppler radar," *J. Atmos. Ocean. Technol.*, vol. 7, no. 2, pp. 255–268, Apr. 1990.

[14] H. W. J. Russchenberg, "Doppler polarimetric radar measurements of the gamma drop size distribution of rain," *J. Appl. Meteorol.*, vol. 32, no. 12, pp. 1815–1825, Dec. 1993.

[15] K. S. Gage and C. R. Williams, "Recent developments in the use of Doppler radar profilers for the remote sensing of precipitating clouds," *Proc. SPIE*, vol. 4894, pp. 293–305, Apr. 2003.

[16] Y. L. Kogan, Z. N. Kogan, and D. B. Mechem, "Assessing the errors of cloud liquid water and precipitation flux retrievals in marine stratocumulus based on Doppler radar parameters," *J. Hydrometeorol.*, vol. 8, no. 4, pp. 665–677, Aug. 2007.

[17] W. Klaassen, "Determination of rain intensity from Doppler spectra of vertically scanning radar," *J. Atmos. Ocean. Technol.*, vol. 6, no. 4, pp. 552–562, Aug. 1989.

[18] J. D. Campbell, K. J. Hutchison, and E. Karpinski, "Variation of Doppler ultrasound spectral width in the post-stenotic velocity field," *Ultrasound Med. Biol.*, vol. 15, no. 7, pp. 611–619, Jan. 1989.

[19] T. Thompson and H. Moore, "A model for Doppler radar echoes from Mars," in *Proc. Lunar Planet. Sci. Conf.*, 1989, pp. 409–422.

[20] G. J. Black, "Planetary radar astronomy," *Single-Dish Radio Astron., Techn. Appl.*, vol. 278, pp. 271–290, Dec. 2002.

[21] T. Dash, O. A. Krasnov, and A. G. Yarovoy, "Performance analysis of the wind field estimation for a very fast scanning weather radar," in *Proc. 23rd Int. Radar Symp. (IRS)*, Sep. 2022, pp. 420–425.

[22] D. Sirmans and B. Bumgarner, "Numerical comparison of five mean frequency estimators," *J. Appl. Meteorol.*, vol. 14, no. 6, pp. 991–1003, Sep. 1975.

[23] P. R. Mahapatra and D. S. ZrniC, "Practical algorithms for mean velocity estimation in pulse Doppler weather radars using a small number of samples," *IEEE Trans. Geosci. Remote Sens.*, vols. GE–21, no. 4, pp. 491–501, Oct. 1983.

[24] D. S. Zrnic, "Spectral moment estimates from correlated pulse pairs," *IEEE Trans. Aerosp. Electron. Syst.*, vol. AES-13, no. 4, pp. 344–354, Jul. 1977.

[25] D. Warde, D. Schvartzman, and C. D. Curtis, "Generalized multi-lag estimators (GMLE) for polarimetric weather radar observations," *IEEE Trans. Geosci. Remote Sens.*, vol. 61, 2023, Art. no. 5105712.

[26] G. Meymaris, J. K. Williams, and J. C. Hubbert, "Performance of a proposed hybrid spectrum width estimator for the NEXRAD ORDA," in *Proc. 25th Conf. Int. Interact. Inf. Process. Syst. Meteorol., Oceanogr. Hydrol.*, 2009, pp. 1–9.

[27] R. Doviak and D. Zrnić, *Doppler Radar and Weather Observations*, 2nd ed. San Diego, CA, USA: Academic, 1993.

[28] J. Lee, "Poly-pulse pair estimation in a Doppler weather radar," in *Proc. IEEE Antennas Propag. Soc., AP-S Int. Symp.*, vol. 4, Jul. 2000, pp. 1968–1971.

[29] J. M. B. Dias and J. M. N. Leitao, "Nonparametric estimation of mean Doppler and spectral width," *IEEE Trans. Geosci. Remote Sens.*, vol. 38, no. 1, pp. 271–282, Jan. 2000.

[30] R. D. Palmer, J. R. Cruz, and D. S. Zrnic', "Enhanced autoregressive moving average spectral estimation applied to the measurement of Doppler spectral width," *IEEE Trans. Geosci. Remote Sens.*, vol. 29, no. 3, pp. 358–368, May 1991.

[31] M. Levin, "Power spectrum parameter estimation," *IEEE Trans. Inf. Theory*, vol. IT-11, no. 1, pp. 100–107, Jan. 1965.

[32] J. M. B. Dias and J. M. N. Leitao, "Maximum likelihood estimation of spectral moments at low signal to noise ratios," in *Proc. IEEE Int. Conf. Acoust. Speech Signal Process.*, 1993, pp. 149–152.

[33] J. Klostermeyer, "Maximum entropy estimation of Doppler shift and spectral width of VHF radar signals," *Radio Sci.*, vol. 24, no. 1, pp. 47–63, Jan. 1989.

[34] P. Waldteufel, "An analysis of weather spectra variance in a tornadic storm," NOAA Tech. Memo ERL NSSL, Nat. Severe Storms Lab., USA, Tech. Rep., 76, 1976.

[35] B. L. Cheong, R. D. Palmer, and M. Xue, "A time series weather radar simulator based on high-resolution atmospheric models," *J. Atmos. Ocean. Technol.*, vol. 25, no. 2, pp. 230–243, Feb. 2008.

[36] P. T. May and R. G. Strauch, "An examination of wind profiler signal processing algorithms," *J. Atmos. Ocean. Technol.*, vol. 6, no. 4, pp. 731–735, Aug. 1989.

[37] W. Rudin, *Principles of Mathematical Analysis*, 3rd ed. New York, NY, USA: McGraw-Hill, 1953.

[38] D. S. Zrnić, "Simulation of weatherlike Doppler spectra and signals," *J. Appl. Meteorol.*, vol. 14, no. 4, pp. 619–620, Jun. 1975.

[39] C. L. Matson and A. Haji, "Biased Cramér-Rao lower bound calculations for inequality-constrained estimators," *J. Opt. Soc. Amer. A, Opt. Image Sci.*, vol. 23, no. 11, pp. 2702–2713, 2006.

[40] P. Stoica and R. Moses, *Spectral Analysis of Signals*, vol. 24, no. 1. Upper Saddle River, NJ, USA: Prentice-Hall, 2008.

[41] T. Liu and D. Li, "Convergence of the BFGS-SQP method for degenerate problems," *Numer. Funct. Anal. Optim.*, vol. 28, nos. 7–8, pp. 927–944, Jul. 2007.

[42] C. G. Broyden, "The convergence of a class of double-rank minimization algorithms 1. General considerations," *IMA J. Appl. Math.*, vol. 6, no. 1, pp. 76–90, 1970.

[43] E. G. Baxa and J. Lee, "The pulse-pair algorithm as a robust estimator of turbulent weather spectral parameters using airborne pulse Doppler radar," NASA, Tech. Rep. NASA-CR-4382, DOT/FAA/RD-91/17, 1991.

[44] H. W. J. Russchenberg and L. P. Ligthart, "Backscattering by and propagation through the melting layer of precipitation: A new polarimetric model," *IEEE Trans. Geosci. Remote Sens.*, vol. 34, no. 1, pp. 3–14, Jan. 1996.

[45] S. Y. Matrosov, "Retrievals of vertical profiles of ice cloud microphysics from radar and IR measurements using tuned regressions between reflectivity and cloud parameters," *J. Geophys. Res., Atmos.*, vol. 104, no. D14, pp. 16741–16753, Jul. 1999.

[46] S. Y. Matrosov and A. J. Heymsfield, "Use of Doppler radar to assess ice cloud particle fall velocity-size relations for remote sensing and climate studies," *J. Geophys. Res., Atmos.*, vol. 105, no. D17, pp. 22427–22436, Sep. 2000.

[47] V. I. Khvorostyanov and J. A. Curry, "Terminal velocities of droplets and crystals: Power laws with continuous parameters over the size spectrum," *J. Atmos. Sci.*, vol. 59, no. 11, pp. 1872–1884, Jun. 2002.

Oleg A. Krasnov received the M.Sc. degree in radio physics from Voronezh State University, Voronezh, Russia, in 1982, and the Ph.D. degree in radio technique from National Aerospace University, "Kharkov Aviation Institute," Kharkiv, Ukraine, in 1994.

In 1999, he joined the International Research Center for Telecommunications and Radar (IRCTR), TU Delft, Delft, The Netherlands. Since 2009, he has been a Senior Researcher at the Microwave Sensing, Signals and Systems (MS3) section of the Faculty of Electrical Engineering, Mathematics, and Computer Science (EEMCS), Delft University of Technology, Delft, and became an Universitair Docent (Assistant Professor) there in 2012. His research interests include radar waveforms, signal and data processing algorithms for polarimetric radars and distributed radar systems, multisensor atmospheric remote sensing, optimal resource management of adaptive radar sensors and distributed systems.

Dr. Krasnov served as the Secretary of the 9th European Radar Conference (EuRAD-2012), Amsterdam, The Netherlands.

Tworit Dash (Graduate Student Member, IEEE) was born in Nayagarh, Odisha, India, in 1994. He received the B.Tech. (Bachelor of Technology) degree from the Department of Instrumentation and Electronics Engineering, College of Engineering and Technology, Bhubaneswar, India, in 2016, and the M.Sc. degree (cum laude) in electrical engineering, telecommunication, and sensing systems track from the Delft University of Technology, Delft, The Netherlands, in 2020.

In September 2020, he joined the Microwave, Sensing, Signals, and Systems Group, Delft University of Technology, as a Ph.D. Student.

Alexander Yarovoy (Fellow, IEEE) received the Diploma degree (Hons.) in radiophysics and electronics and the Candidate Phys. and Math.Sci. and Doctor Phys. and Math.Sci. degrees in radiophysics from Kharkov State University, Kharkiv, Ukraine, in 1984, 1987, and 1994, respectively.

In 1987, he joined the Department of Radiophysics, Kharkov State University, as a Researcher, where he became a Professor in 1997. From September 1994 to 1996, he was with the Technical University of Ilmenau, Ilmenau, Germany, as a Visiting Researcher. Since 1999, he has been with the Delft University of Technology, Delft, The Netherlands. Since 2009, he has been leading the Chair of Microwave Sensing, Systems and Signals. He has authored or coauthored more than 450 scientific or technical articles, four patents, and 14 book chapters. His main research interests are in high-resolution radar, microwave imaging, and applied electromagnetics (in particular, UWB antennas).

Dr. Yarovoy was a recipient of the European Microwave Week Radar Award for the paper that best advances the state of the art in radar technology in 2001 (together with L.P. Ligthart and P. van Genderen) and in 2012 (together with T. Savelyev). In 2010, together with D. Caratelli, he received the Best Paper Award from the Applied Computational Electromagnetic Society (ACES). He served as the General TPC Chair of the 2020 European Microwave Week (EuMW'20), the Chair and the TPC Chair of the Fifth European Radar Conference (EuRAD'08), and the Secretary of the First European Radar Conference (EuRAD'04). He also served as the Co-Chair and the TPC Chair of the Xth International Conference on GPR (GPR2004). He served as a Guest Editor for five special issues of IEEE TRANSACTIONS and other journals. Since 2011, he has been an Associate Editor of the *International Journal of Microwave and Wireless Technologies*. From 2008 to 2017, he served as the Director for the *European Microwave Association* (EuMA).

Hans Driessen received the M.Sc. and Ph.D. degrees from the Department of Electrical Engineering, TU-Delft, Delft, The Netherlands, in 1987 and 1992, respectively.

Since then he has been employed with Thales Nederland BV, Hengelo, The Netherlands. He has held various positions as a System Designer of plot extraction and track processing, technical authority on tracking and data fusion, and knowledge and technology manager in the area of algorithms for radar signal/data processing and radar management. He has been involved in the acquisition, execution, and monitoring of a variety of (inter)national research projects, including EDA and EU FP6/7 projects. He holds a partime position as an Associate Professor in the field of radar systems, waveforms, and processing at EEMCS Faculty, Microwave Signals Sensor and Systems Group.